CLASS INCREMENTAL LEARNING VIA LIKELIHOOD RATIO BASED TASK PREDICTION

Haowei Lin¹, Yijia Shao², Weinan Qian³, Ningxin Pan³, Yiduo Guo³, and Bing Liu^{4*}

ABSTRACT

Class incremental learning (CIL) is a challenging setting of continual learning, which learns a series of tasks sequentially. Each task consists of a set of unique classes. The key feature of CIL is that no task identifier (or task-id) is provided at test time for each test sample. Predicting the task-id for each test sample is a challenging problem. An emerging theoretically justified and effective approach is to train a task-specific model for each task in a shared network for all tasks based on a task-incremental learning (TIL) method to deal with forgetting. The model for each task in this approach is an out-of-distribution (OOD) detector rather than a conventional classifier. The OOD detector can perform both within-task (in-distribution (IND)) class prediction and OOD detection. The OOD detection capability is the key for task-id prediction during inference for each test sample. However, this paper argues that using a traditional OOD detector for task-id prediction is sub-optimal because additional information (e.g., the replay data and the learned tasks) available in CIL can be exploited to design a better and principled method for task-id prediction. We call the new method TPLR (Task-id Prediction based on Likelihood Ratio). TPLR markedly outperforms strong CIL baselines.

1 Introduction

Continual learning (CL) learns a sequence of tasks, $1, 2, \dots, T$, incrementally (De Lange et al., 2021; Wang et al., 2023). Each task t consists of a set of classes to be learned. This paper focuses on the challenging CL setting of class-incremental learning (CIL) (Rebuffi et al., 2017). The key challenge of CIL lies in the absence of task-identifier (task-id) in testing. There is another CL setting termed task-incremental learning (TIL), which learns a separate model or classifier for each task. In testing, the task-id is provided for each test sample so that it is classified by the task specific model.

A main assumption of CL is that once a task is learned, its training data is no longer accessible. This causes the problem of *catastrophic forgetting* (CF), which refers to performance degradation of previous tasks due to parameter updates in learning each new task (McCloskey & Cohen, 1989). An additional challenge specifically for CIL is *inter-task class separation* (ICS) (Kim et al., 2022b). That is, when learning a new task, it is hard to establish decision boundaries between the classes of the new task and the classes of the previous tasks without the training data of the previous tasks. Although in replay-based methods (Rebuffi et al., 2017; Kemker & Kanan, 2017; Lopez-Paz & Ranzato, 2017), a small number of training samples can be saved from each task (called the *replay data*) to help deal with CF and ICS to some extent by jointly training the new task data and the replay data from previous tasks, the effect on CF and ICS is limited as the number of replay samples is very small.

An emerging theoretically justified approach to solving CIL is to combine a TIL technique with an out-of-distribution (OOD) detection method, called the TIL+OOD approach. The TIL method learns a model for each task in a shared notwork. The model for each task is not a traditional classifier but an

¹Institute for Artificial Intelligence, Peking University ²Stanford University

³Wangxuan Institute of Computer Technology, Peking University

⁴Department of Computer Science, University of Illinois at Chicago

¹linhaowei@pku.edu.cn ²shaoyj@stanford.edu

³{ypqwn, 2100017816}@stu.pku.edu.cn ⁴liub@uic.edu

^{*}Correspondance author. Bing Liu liub@uic.edu>

Our code is publicly available at https://github.com/linhaowei1/TPLR.

OOD detector. Note that almost all OOD detection methods can perform two tasks (1) *in-distribution* (IND) classification and (2) *out-of-distribution* (OOD) detection (Vaze et al., 2022). At test time, for each test sample, the system first predicts the task (task-id) that the test sample belongs to, which is called the *task-id prediction* (TP) and the task specific model is then used to classify the test sample, which is called *within-task prediction* (WP) (Kim et al., 2022b) (same as IND classification). WP is usually very accurate because it uses the task specific model. **TP is the key challenge**.

The general approach of first predicting task-id (TP) and then predicting the class (WP) of the test sample using the task specific model is not new. Several prior systems have used this approach (Rajasegaran et al., 2020; Abati et al., 2020; Von Oswald et al., 2019). However, what is new is that Kim et al. (2022b) theoretically proved that TP is correlated with OOD detection of each task as they bound each other. Thus, the OOD detection capability of each task model can be used for task-id prediction (TP) of each test sample. The previous methods did not realize this and thus performed poorly (Kim et al., 2022b). In Kim et al. (2022b), the authors used the TIL method HAT (Serra et al., 2018) and OOD detection method CSI (Tack et al., 2020). HAT is a parameter isolation method for TIL, which learns a model for each task in a shared network and each task model is protected with learned masks to overcome CF. Each task model is an OOD detector based on CSI.²

This paper argues that using a traditional OOD detector is not optimal for TP as they are not designed for CIL and thus do not exploit the information available in CIL for better task-id prediction. By leveraging the information in the CIL process, we can do much better. A new method for task-id prediction is proposed, which we call **TPLR** (*Task-id Prediction based on Likelihood Ratio*). It consists of two parts: (1) a different method to train each task model and (2) a novel and principled method for task-id prediction, i.e., to estimate the probability of a test sample x belonging to a task t, i.e., P(t|x)). We formulate the estimation of P(t|x) as a binary selection problem between two events "x belongs to t" and "x belongs to t". t0 is t0 s complement with regard to the universal set t1, which consists of all tasks that have been learned, i.e., t2 and t3 and t4 and t5.

The idea of TPLR is analogous to using OOD detection for task-id prediction in the previous work. However, there is a **crucial difference**. In traditional OOD detection, given a set U_{IND} of in-distribution classes, we want to estimate the probability that a test sample does not belong to any classes in U_{IND} . This means the universal set U_{OOD} for OOD detection includes all possible classes in the world (except those in U_{IND}), which is at least very large if not infinite in size and we have no data from U_{OOD} . Then, there is no way we can estimate the distribution of U_{OOD} . However, we can estimate the distribution of U_{CIL} based on the saved replay data from each task in CIL. This allows us to use the *likelihood ratio* of \mathcal{P}_t and \mathcal{P}_{t^c} to provide a principled solution towards the binary selection problem and consequently to produce the task-id prediction probability $\mathbf{P}(t|\mathbf{x})$ as analysed in Section 4.1, where \mathcal{P}_t is the distribution of the data in task t and \mathcal{P}_{t^c} is the distribution of the data in t^c (all other tasks than t), i.e., t's complement ($t^c = U_{CIL} - \{t\}$).

The proposed whole system (which we also call TPLR) also uses the learned masks in the TIL method HAT for overcoming CF but the model for each task within the HAT structure is not a traditional classifier as in the original HAT. It is a model that can facilitate task-id prediction (detailed in Section 3). At test time, given a test sample, the proposed likelihood ratio method is integrated with a logit-based score using an energy function to compute the task-id prediction (TP) probability and within-task prediction (WP) probability for the test sample to finally predict its class. Extensive experiments with and without using a pre-trained feature extractor show that the proposed method markedly outperforms the state-of-the-art baselines.

2 Related Work

OOD Detection. OOD detection has been studied extensively. For example, using the maximum softmax probability (MSP) as the OOD score is proposed in Hendrycks & Gimpel (2016). More advanced methods exploit the logit space (Liang et al., 2017; Liu et al., 2020a; Sun et al., 2021; Hendrycks et al., 2019), and the feature space to compute the distance from the test sample to the training data/IND distribution, e.g., Mahalanobis distance (Lee et al., 2018b) and KNN (Sun et al., 2022). Some systems also use real/generated OOD data (Liu et al., 2020a; Lee et al., 2018a; Wang et al., 2022d). For comprehensive surveys, please refer to Yang et al. (2021); Cui & Wang (2022). As discussed in the introduction, our task-id prediction does not use traditional OOD detection.

²In Kim et al. (2023), it was also shown that based on this approach, CIL is learnable.

Continual Learning (CL). Existing CL methods can be roughly categorized into three groups. The first group comprises *regularization-based* methods, which address forgetting (CF) by using regularization terms in the loss function (Zhu et al., 2021) or orthogonal projection (Zeng et al., 2019) to preserve previous important parameters. *Replay-based* methods are the second group, which save a few samples from each task to rehearse past knowledge during training for new tasks (Kemker & Kanan, 2017; Lopez-Paz & Ranzato, 2017; Li et al., 2022). The third group is *parameter isolation*, which trains a sub-network for each task (Serra et al., 2018; Wortsman et al., 2020; Mallya & Lazebnik, 2018; Ke et al., 2022). HAT (Serra et al., 2018) and SupSup (Wortsman et al., 2020) are two representative methods. This approach is commonly used in task-incremental learning (TIL), which has almost no CF for TIL. DER (Yan et al., 2021) and BEEF Wang et al. (2022a) for CIL are also related but they expand the network for each task. Their regularizations are similar to OOD detection. As we will see in Section 5.2, their results are markedly poorer than the proposed method.

Recently, using pre-trained models has become a standard practice for CL in both computer vision (CV) (Kim et al., 2022a; Wang et al., 2022e) and NLP (Ke et al., 2021a;b; 2022). See the surveys (De Lange et al., 2021; Hadsell et al., 2020; Biesialska et al., 2020) for additional information.

As discussed in the introduction section, our work is closely related to the CIL methods that employ a TIL technique in conjunction with an additional task-id prediction mechanism. For instance, iTAML (Rajasegaran et al., 2020) mandates that each test batch originates from a single task and uses the whole batch of data to detect the task-id, which is impractical as test samples are typically received individually. CCG (Abati et al., 2020) devises a separate network to predict the task-id, while Expert Gate (Aljundi et al., 2017) constructs a distinct auto-encoder for each task. HyperNet (Von Oswald et al., 2019) and PR-Ent (Henning et al., 2021) utilize entropy as a means of task-id prediction. However, these systems perform poorly (Kim et al., 2022b) as they did not realize that OOD detection is the key to task-id prediction. Based on the idea of using a TIL method and an OOD method (i.e., TIL+OOD), Kim et al. (2022b) proposed two methods HAT+CSI (which is the combination of the existing TIL method HAT (Serra et al., 2018) and the OOD detection method CSI (Tack et al., 2020)) and SupSup+CSI (Kim et al., 2022b) (which is the combination of the TIL method SupSup (Wortsman et al., 2020) and CSI). These two methods do not use a pre-trained model or replay data. The same approach was also taken in MORE (Kim et al., 2022a) and ROW (Kim et al., 2023) but they employ a pre-trained model and replay data in CIL. These methods have established a state-of-the-art performance. We have discussed how our proposed method TPLR is different from them in the introduction section. Our experimental results also show that the proposed TPLR method significantly outperforms these existing methods.

3 OVERVIEW OF THE PROPOSED METHOD

Preliminary. Class incremental learning (CIL) learns a sequence of tasks 1,...,T. Each task t has an input space $\mathcal{X}^{(t)}$, a label space $\mathcal{Y}^{(t)}$, and a training set $\mathcal{D}^{(t)} = \{(\boldsymbol{x}_j^{(t)}, y_j^{(t)})\}_{j=1}^{n^{(t)}}$ drawn i.i.d. from $\mathcal{P}_{\mathcal{X}^{(t)}\mathcal{Y}^{(t)}}$. The class labels of the tasks are disjoint, i.e., $\mathcal{Y}^{(i)} \cap \mathcal{Y}^{(k)} = \emptyset, \forall i \neq k$. The goal of CIL is to learn a function $f: \cup_{t=1}^T \mathcal{X}^{(t)} \to \cup_{t=1}^T \mathcal{Y}^{(t)}$ to predict the class label of each test sample \boldsymbol{x} .

Kim et al. (2022b) proposed a theoretical framework for solving CIL. It decomposes the CIL probability of a test sample x of the j-th class $y_j^{(t)}$ in task t into two probabilities (as the classes in all tasks are disjoint),

$$\mathbf{P}(y_j^{(t)}|\mathbf{x}) = \mathbf{P}(y_j^{(t)}|\mathbf{x}, t)\mathbf{P}(t|\mathbf{x}). \tag{1}$$

The two probabilities on the right-hand-side (R.H.S) define the CIL probability on the left-hand-side (L.H.S). The first probability on the R.H.S. is the *within-task prediction* (**WP**) probability and the second probability on the R.H.S. is the *task-id prediction* (**TP**) probability. Existing methods basically use a traditional OOD detection method to build each task model. The OOD detection model for each task is exploited for estimating both TP and WP probabilities (see Section 1).

Overview of the Proposed TPLR

This paper focuses on proposing a novel method for estimating task-id prediction probability, i.e., the probability of a test sample \boldsymbol{x}) belonging to (or drawing from the distribution of) a task t, i.e., $\mathbf{P}(t|\boldsymbol{x})$ in eq. (1). The WP probability $\mathbf{P}(y_i^{(t)}|\boldsymbol{x},t)$ can obtained directly from the model of each task.

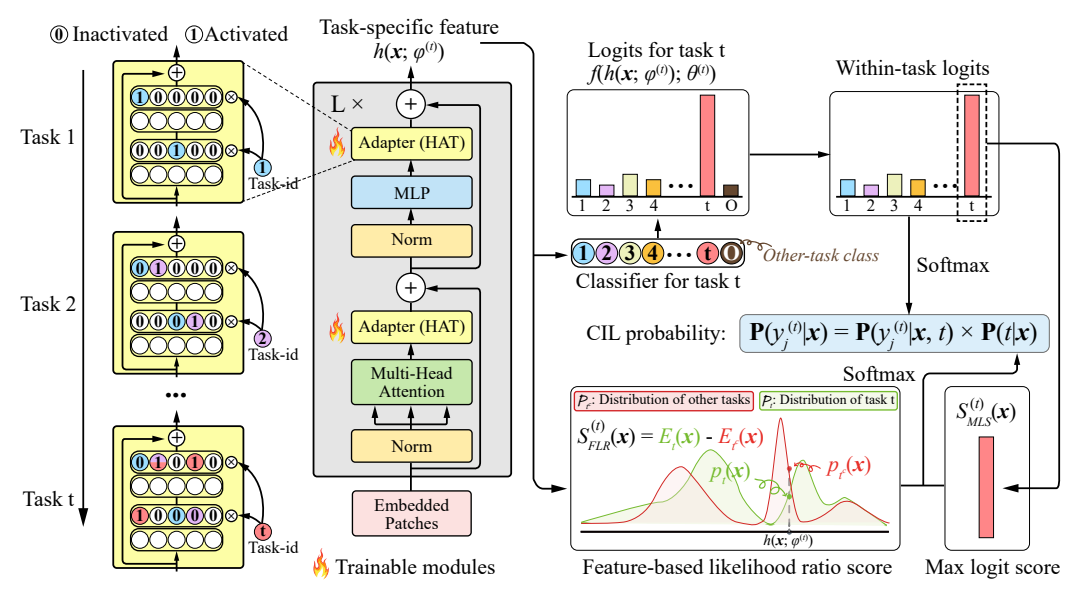


Figure 1: Illustration of the proposed TPLR. We use a pre-trained transformer network (in the grey box) (see Section 5.1 for the case without using a pre-trained network). The pre-trained network is fixed and only the adapters (Houlsby et al., 2019) inserted into the transformer are trainable or tunnable to adapt to specific tasks. It is important to note that the adapter (in yellow) used by HAT learns all tasks within the same adapter. The yellow boxes on the left shows the progressive changes to the adapter as more tasks are learned.

The mask-based approach in the TIL method HAT (Serra et al., 2018) is used by our method to prevent CF. Briefly, HAT learns a sequence of tasks incrementally. In learning each task, apart from learning a model for the task, a set of masks is also learned at the same time for those important neurons of the model to be used later to prevent the model from being updated by future tasks. In learning a new task, the masks for previous task models will stop the gradient flow to those masked neurons in back-propagation, which effectively eliminate CF. In the forward pass, all the neurons can be used, so the network is shared by all tasks.

The proposed method TPLR is illustrated in Figure 1. It has two techniques for accurate estimation of $\mathbf{P}(t|\mathbf{x})$, one in training and one in testing (inference).

(1) **Training**: In the original HAT, each model is a traditional supervised classifier trained with cross-entropy. However, for our purpose of predicting task-id, this is insufficient because it has no consideration of the other classes learned from other tasks. In TPLR, each model for a task t is trained using the classes $\mathcal{Y}^{(t)}$ of task t and an extra class (called O, for others) representing the replay buffer data $Buf_{< t}$ of all the previous tasks. This enables each model to consider not only the new task data but also previous tasks data, which facilitates more accurate computation of $\mathbf{P}(t|\mathbf{x})$. This O class is not used in inference. In inference, the WP probability $(\mathbf{P}(y_j^{(t)}|\mathbf{x},t))$ for each test sample is computed through softmax on only the original classes $\mathcal{Y}^{(t)}$ of task t.

For each task t, its model consists of a feature extractor $h(\boldsymbol{x}; \phi^{(t)})$ (partially shared with other tasks based on HAT), and a task-specific classifier $f(\boldsymbol{z}; \theta^{(t)})$. When learning task t, the model receives the training data $\mathcal{D}^{(t)}$ and the replay data $Buf_{\leq t}$ (stored in a memory buffer). Then we minimize the loss:

$$\mathcal{L}(\theta^{(t)}, \phi^{(t)}) = \mathbb{E}_{(\boldsymbol{x}, y) \sim \mathcal{D}^{(t)} \cup Buf_{< t}} \left[\mathcal{L}_{CE}(f(h(\boldsymbol{x}; \phi^{(t)}); \theta^{(t)}), y) \right] + \mathcal{L}_{HAT}, \tag{2}$$

where \mathcal{L}_{CE} is the cross-entropy loss, \mathcal{L}_{HAT} is the regularization loss used in HAT (see Appendix E).

(2) **Testing (or inference)**: We follow eq. (1) to compute the CIL probability. The WP probability $\mathbf{P}(y_j^{(t)}|\boldsymbol{x},t)$ can be estimated by the classifier (the first term on the right of eq. (3) below, and see the top right part in Figure 1).

$$\mathbf{P}(y_j^{(t)}|\boldsymbol{x}) = \left[softmax\left(f(h(\boldsymbol{x};\phi^{(t)});\theta^{(t)})\right)\right]_j \cdot \mathbf{P}(t|\boldsymbol{x}) \tag{3}$$

The class $y_j^{(t)}$ with the highest probability will be predicted as the class for test sample x.³ We discuss the proposed method for computing task-id prediction probability $\mathbf{P}(t|x)$ (see the bottom right part in Figure 1) in the next section. Training will not be discussed any further.

4 ESTIMATING TASK-ID PREDICTION PROBABILITY

4.1 THEORETICAL ANALYSIS

As noted in Section 1, we estimate the TP probability $\mathbf{P}(t|\mathbf{x})$ by predicting whether a sample \mathbf{x} is drawn from the distribution \mathcal{P}_t of task t or drawn from the distribution of t's complement t^c , i.e., \mathcal{P}_{t^c} . We denote the universal set U_{CIL} of all tasks (or task-ids) that have been learned, i.e., $U_{CIL} = \{1, 2, \cdots, T\}$ and $t^c = U_{CIL} - \{t\}$. From a frequentist perspective, our objective can be formulated as a binary hypothesis test:

$$\mathcal{H}_0: \boldsymbol{x} \sim \mathcal{P}_t \quad v.s. \quad \mathcal{H}_1: \boldsymbol{x} \sim \mathcal{P}_{t^c},$$
 (4)

Using the Neyman-Pearson lemma (Neyman & Pearson, 1933), we can derive a theorem that demonstrates the principled role of likelihood ratio in this task (the proofs are given in Appendix C):

Theorem 4.1 A test with rejection region \mathbb{R} defined as follows is a unique uniformly most powerful *(UMP)* test for the hypothesis test problem defined in eq. (4):

$$\mathcal{R} := \{ \boldsymbol{x} : p_t(\boldsymbol{x}) / p_{t^c}(\boldsymbol{x}) < \lambda_0 \}.$$

where λ_0 is a threshold that can be chosen to obtain a specified significance level.

Theorem 4.2 The UMP test for hypothesis test defined in eq. (4) maximizes the Area Under the Curve (AUC) of binary classification between \mathcal{P}_t and \mathcal{P}_{t^c} .

Theorems 4.1 and 4.2 highlight the importance of detecting samples that do not belong to task t based on low t density $p_t(\mathbf{x})$ and high t^c density $p_{t^c}(\mathbf{x})$.

Note that in traditional OOD detection, the system has no access to the true OOD distribution \mathcal{P}_{t^c} but only \mathcal{P}_t (IND distribution). Some existing methods resort to a proxy distribution $\mathcal{P}_{t^c}^{proxy}$, such as a uniform distribution (Nalisnick et al., 2018) or an auxiliary data distribution (Hendrycks et al., 2018) as the universal set U is the set of all classes in the world and the universal set of all OOD classes for task t denoted by $U_{OOD}^{(t)}$ is very large if not infinite. This approach can lead to potential risks. For instance, consider a scenario where $\mathcal{P}_{t^c} = \mathcal{N}(0,0.01)$ and $\mathcal{P}_t = \mathcal{N}(0,1)$. It is apparent that $p_t(0) > p_t(1)$, but 0 is more likely to belongs to \mathcal{P}_{t^c} than 1 as $0.1 = p_t(0)/p_{t^c}(0) < p_t(1)/p_{t^c}(1) = 0.1 \cdot \mathrm{e}^{49.5}$. Therefore, an accurate estimate of \mathcal{P}_{t^c} is important.

Good News for CIL. In CIL, the IND distribution \mathcal{P}_t for task t can be interpreted as the marginal distribution $\mathcal{P}_{\mathcal{X}^{(t)}}$, while \mathcal{P}_{t^c} corresponds to a mixture distribution $\mathcal{P}_{\mathcal{X}^{(t^c)}}$ comprising the individual marginal distributions $\{\mathcal{P}_{\mathcal{X}^{(t^*)}}\}_{t^* \neq t}$ (which can be estimated based on the saved replay data), each of which is assigned the equal mixture weight. Consequently, we have the knowledge of \mathcal{P}_{t^c} in CIL, thereby offering an opportunity to estimate \mathcal{P}_{t^c} to be used to compute task-id prediction $\mathbf{P}(t|\mathbf{x})$ more accurately. This leads to our design of TPLR in the following subsections.

4.2 Computing Task-ID Prediction Probability

We now present the proposed method for computing the task-id prediction probability $\mathbf{P}(t|\mathbf{x})$, which has three parts: (1) estimating both \mathcal{P}_t and \mathcal{P}_{t^c} (as analyzed in Section 4.1) and computing the likelihood ratio, (2) integrating the likelihood ratio based score with a logit-based score for further improvement, and (3) applying a softmax function on the scores for all tasks to obtain the task-id prediction probability for each task.

³We also develop a calibration method detailed in Appendix A to calibrate the probabilities from different task models, but it has little effect on the final performance.

4.2.1 ESTIMATING \mathcal{P}_t AND \mathcal{P}_{t^c} AND COMPUTING LIKELIHOOD RATIO

Guided by Theorem 4.1, we design a task-id prediction score based on the likelihood ratio $p_t(x)/p_{t^c}(x)$. However, due to the challenges in directly estimating the data distribution within the high-dimensional raw image space, we instead consider estimation in the low-dimensional *feature space*. Interestingly, many distance-based OOD detection scores can function as density estimators that estimate the IND density p(x) in the *feature space* (see Appendix C.4 for justifications). For instance, MD (*Mahalanobis Distance*) (Lee et al., 2018b) estimates distributions using Gaussian mixture models, while KNN (Sun et al., 2022) uses non-parametric estimation. Our method TPLR also uses the two scores to estimate distributions (i.e., \mathcal{P}_t and \mathcal{P}_{t^c} in our case).

To connect the normalized probability density with unnormalized task-id prediction scores, we leverage energy-based models (EBMs) to parameterize \mathcal{P}_t and \mathcal{P}_{t^c} . Given a test sample \boldsymbol{x} , it has density $p_t(\boldsymbol{x}) = \exp\{E_t(\boldsymbol{x})\}/Z_1$ in \mathcal{P}_t , and density $p_{t^c}(\boldsymbol{x}) = \exp\{E_{t^c}(\boldsymbol{x})\}/Z_2$ in \mathcal{P}_{t^c} , where Z_1, Z_2 are normalization constants that ensure the integral of densities $p_t(\boldsymbol{x})$ and $p_{t^c}(\boldsymbol{x})$ equal 1, and $E_t(\cdot), E_{t^c}(\cdot)$ are called *energy functions*. Consequently, we can design a feature-based task-id prediction score using the Likelihood Ratio (LR):

$$S_{LR}^{(t)}(\mathbf{x}) = \log(p_t(\mathbf{x})/p_{t^c}(\mathbf{x})) = E_t(\mathbf{x}) - E_{t^c}(\mathbf{x}) + \log(Z_2/Z_1).$$
 (5)

Since $\log(Z_2/Z_1)$ is a constant, it can be omitted in the task-id prediction score definition:

$$S_{LR}^{(t)}(\boldsymbol{x}) := E_t(\boldsymbol{x}) - E_{t^c}(\boldsymbol{x}), \tag{6}$$

Since the energy functions $E_t(\cdot)$ and $E_{t^c}(\cdot)$ need not to be normalized, we estimate them with the above scores. We next discuss how to choose specific $E_t(\cdot)$ and $E_{t^c}(\cdot)$ for eq. (6).

For in-task energy $E_t(\boldsymbol{x})$ of a task, we simply adopt an OOD detection score $S_{MD}(\boldsymbol{x})$, which is the OOD score for MD and is defined as the inverse of the minimum Mahalanobis distance of feature $h(\boldsymbol{x};\phi^{(t)})$ to all class centroids. The details of how $S_{MD}^{(t)}(\boldsymbol{x})$ is computed are given in Appendix D.1.

For out-of-task energy $E_{t^c}(\boldsymbol{x})$ of a task, we use **replay data** from other tasks for estimation. Let Buf_{t^c} be the set of buffer/replay data excluding the data of classes in task t. We set $E_{t^c}(\boldsymbol{x}) = -d_{KNN}(\boldsymbol{x}, Buf_{t^c})$, where $d_{KNN}(\boldsymbol{x}, Buf_{t^c})$ is the k-nearest distances of the feature $h(\boldsymbol{x}; \phi)^{(t)}$ to the set of features of the replay Buf_{t^c} data. If $d_{KNN}(\boldsymbol{x}, Buf_{t^c})$ is small, it means the distance between \boldsymbol{x} and replay Buf_{t^c} data is small in the feature space. The vanilla KNN score is $S_{KNN}^{(t)}(\boldsymbol{x}) = -d_{KNN}(\boldsymbol{x}, \mathcal{D}^{(t)})$, which was originally designed to estimate $p_t(\boldsymbol{x})$ using the training set $\mathcal{D}^{(t)}$. Here we adopt it to estimate $p_{t^c}(\boldsymbol{x})$ using the replay data (Buf_{t^c}) . Finally, we obtain,

$$S_{LR}^{(t)}(\boldsymbol{x}) := \underbrace{\alpha \cdot S_{MD}^{(t)}(\boldsymbol{x})}_{E_t(\boldsymbol{x})} + \underbrace{d_{KNN}(\boldsymbol{x}, Buf_{t^c})}_{-E_{t^c}(\boldsymbol{x})}, \tag{7}$$

where α is a hyper-parameter to make the two scores comparable. This is a principled task-id prediction score as justified in Section 4.1.

Remarks. We can also use some other feature-based estimation methods instead of MD and KNN in $S_{LR}(x)$. The reason why we choose MD to estimate \mathcal{P}_t is that it does not require the the task data at test time (but KNN does), and we choose KNN to estimate \mathcal{P}_{t^c} because the non-parametric estimator KNN is high performing (Yang et al., 2022) and we use only the saved replay data for this. We will conduct an ablation study using different estimation methods for both \mathcal{P}_t and \mathcal{P}_{t^c} in Section 5.3.

4.2.2 Combining with a Logit-Based Score

To further improve the task-id prediction score, we combine the feature-based S_{LR} score with a logit based score, which has been shown quite effective in OOD detection (Wang et al., 2022c).

We again develop an energy-based model (EBM) framework for the combination that offers a principled approach to composing different task-id prediction scores. Specifically, to combine the

⁴In EBMs, the density p(x) is typically defined as $\exp\{-E(x)\}/Z$. Since our task-id prediction score is defined to measure the likelihood that the test sample belongs to a task, the energy function here is defined positively related to the probability density.

proposed feature-based $S_{LR}^{(t)}(\cdot)$ score with a logit-based score (an energy function) $S_{logit}^{(t)}(\cdot)$, we can make the composition as:

$$E_{composition}(\boldsymbol{x}) = \log(\exp\{\alpha_1 \cdot S_{logit}^{(t)}(\boldsymbol{x})\} + \exp\{\alpha_2 \cdot S_{LR}^{(t)}(\boldsymbol{x})\}), \tag{8}$$

where α_1 and α_2 are scaling terms to make different scores comparable. As noted in Du et al. (2020), the composition emulates an OR gate for energy functions.

To choose a logit-based method for $S_{logit}^{(t)}(\cdot)$ in eq. (8), we opt for the simple yet effective method MLS score $S_{MIS}^{(t)}(\boldsymbol{x})$, which is defined as the *maximum logit* of \boldsymbol{x} .

Our final score $S_{TPLR}^{(t)}(\boldsymbol{x})$, which integrates feature-based $S_{LR}^{(t)}(\cdot)$ and the logit-based $S_{MLS}^{(t)}(\cdot)$ scores, uses the composition in Eq. 8:

$$S_{TPLR}^{(t)}(\boldsymbol{x}) = \log \left(\exp\{\beta_1 \cdot S_{MLS}^{(t)}(\boldsymbol{x})\} + \exp\{\beta_2 \cdot S_{MD}^{(t)}(\boldsymbol{x}) + d_{KNN}(\boldsymbol{x}, Buf_{t_c})\} \right), \tag{9}$$

where β_1 and β_2 are scaling terms, which are given by merging α in eq. (7) and α_1 , α_2 in eq. (8). Since the scale of $d_{KNN}(\cdot)$ is near to 1, we simply choose β_1 and β_2 to be the inverse of empirical means of $S_{MLS}^{(t)}(\boldsymbol{x})$ and $S_{MD}^{(t)}(\boldsymbol{x})$ estimated by the training data $\mathcal{D}^{(t)}$ to make different scores comparable:

$$\frac{1}{\beta_1} = \frac{1}{|\mathcal{D}^{(t)}|} \sum_{\boldsymbol{x} \in \mathcal{D}^{(t)}} S_{MLS}^{(t)}(\boldsymbol{x}), \quad \frac{1}{\beta_2} = \frac{1}{|\mathcal{D}^{(t)}|} \sum_{\boldsymbol{x} \in \mathcal{D}^{(t)}} S_{MD}^{(t)}(\boldsymbol{x})$$
(10)

Remarks. We exploit **EBMs**, which are known for their *flexibility* but suffering from *tractability*. However, we exploit EBMs' *flexibility* to derive principled task-id prediction score following Theorem 4.1 and eq. (8), while keep the *tractability* via approximation using OOD scores (MD, KNN, MLS) in practice. This makes our proposed TPLR maintains both theoretical and empirical soundness.

4.3 Converting Task-id Prediction Scores to Probabilities

Although theoretically principled as shown in Section 4.1, our final task-id prediction score is still an unnormalized energy function. We convert the task-id prediction scores for all tasks (i.e., $\{S_{TPLR}^{(t)}(x)\}_{t=1}^T$) to normalized probabilities via softmax:

$$\mathbf{P}(t|\mathbf{x}) = softmax \left(\left[S_{TPLR}^{(1)}(\mathbf{x}), S_{TPLR}^{(2)}(\mathbf{x}), \cdots, S_{TPLR}^{(T)}(\mathbf{x}) \right] / \gamma \right)_t, \tag{11}$$

where γ is a temperature parameter. To encourage confident task-id prediction, we set a low temperature $\gamma=0.05$ to produce a low entropy task-id prediction distribution for all our experiments.

5 EXPERIMENTS

5.1 EXPERIMENTAL SETUP

CIL Baselines. We compare our TPLR system with 17 baselines, which include 11 replay-based methods: iCaRL (Rebuffi et al., 2017), A-GEM (Chaudhry et al., 2018), EEIL (Castro et al., 2018), GD (Lee et al., 2019), DER++ (Buzzega et al., 2020), HAL (Chaudhry et al., 2021), DER (Yan et al., 2021), FOSTER (Wang et al., 2022b), BEEF (Wang et al., 2022a), MORE (Kim et al., 2022a), ROW (Kim et al., 2023), and 6 non-reply methods: HAT (Serra et al., 2018), ADAM (Zhou et al., 2023), OWM (Zeng et al., 2019), PASS (Zhu et al., 2021), SLDA (Hayes & Kanan, 2020), and L2P (Wang et al., 2022e). Implementation details, network size and running time are given in Appendix F.1.

Datasets. To form a sequence of tasks in CIL experiments, we follow the common CIL setting. We split CIFAR-10 into 5 tasks (2 classes per task) (C10-5T). For CIFAR-100, we conduct two experiments: 10 tasks (10 classes per task) (C100-10T) and 20 tasks (5 classes per task) (C100-20T).

⁵The systems HAT+CSI and Sup+CSI in (Kim et al., 2022b) (which are based on the TIL+OOD paradigm but do not use a pre-trained model) are not included as they are much weaker (up to 21% lower than TPLR in accuracy) because their approach of using contrastive learning and data augmentations does not work well with a pre-trained model.

Table 1: CIL ACC (%). "-XT": X number of tasks. The best result in each column is highlighted in bold. The baselines are divided into two categories via dashed lines. The first category contains non-replay methods, and the second category contains replay-based methods. **Upper Bound** denotes pooling all tasks together to learn all classes as one task, which gives the performance upper bound for CIL. **Avg** means the average incremental ACC (%). **Last** is the ACC after learning the final task. See **forgetting rate results** in Appendix B.1.

	C1	0-5T	C100)-10T	C100)-20T	T-	5T	T-	10T	Ave	rage
	Last	Avg	Last	Avg	Last	Avg	Last	Avg	Last	Avg	Last	Avg
Upper Bound	95.79 ^{±0.15}	$97.01^{\pm0.14}$	$82.76^{\pm0.22}$	$87.20^{\pm0.29}$			$72.52^{\pm0.41}$	$77.03^{\pm0.47}$	$72.52^{\pm0.41}$	$77.03^{\pm0.41}$	83.70	85.16
OWM	41.69 ^{±6.34}	$56.00^{\pm3.46}$	$21.39^{\pm3.18}$	$40.10^{\pm 1.86}$	$16.98^{\pm 4.44}$	$32.58^{\pm1.58}$	$24.55^{\pm 2.48}$	$45.18^{\pm0.33}$	$17.52^{\pm3.45}$	$35.75^{\pm 2.21}$	24.43	41.92
ADAM	83.92 ^{±0.51}	$90.33^{\pm0.42}$	$61.21^{\pm0.36}$		$58.99^{\pm0.61}$	$70.89^{\pm0.51}$	$50.11^{\pm0.46}$	$61.85^{\pm0.51}$	$49.68^{\pm0.40}$		60.78	71.41
PASS	86.21 ^{±1.10}		$68.90^{\pm0.94}$			$76.42^{\pm1.23}$	$61.03^{\pm0.38}$	$67.12^{\pm 6.26}$	$58.34^{\pm0.42}$	$67.33^{\pm 3.63}$	68.25	75.38
HAT	82.40 ^{±0.12}	$91.06^{\pm0.36}$	$62.91^{\pm0.24}$		$59.54^{\pm0.41}$	$69.12^{\pm 1.06}$	$59.22^{\pm0.10}$	$69.38^{\pm1.14}$		$65.63^{\pm 1.64}$	63.62	73.84
SLDA	88.64 ^{±0.05}	$93.54^{\pm0.66}$	$67.82^{\pm0.05}$			$78.51^{\pm0.58}$		$66.03^{\pm 1.35}$	$57.93^{\pm0.06}$	$67.39^{\pm1.81}$	68.02	76.64
L2P	73.59 ^{±4.15}	$84.60^{\pm 2.28}$	$61.72^{\pm0.81}$	$72.88^{\pm1.18}$	53.84 ^{±1.59}	$66.52^{\pm 1.61}$	$59.12^{\pm0.96}$	67.81 ^{±1.25}	$54.09^{\pm 1.14}$	64.59 ^{±1.59}	60.47	71.28
iCaRL	87.55 ^{±0.99}	$89.74^{\pm 6.63}$	$68.90^{\pm0.47}$	$76.50^{\pm3.56}$	$69.15^{\pm0.99}$	$77.06^{\pm2.36}$	$53.13^{\pm 1.04}$	$61.36^{\pm6.21}$	$51.88^{\pm 2.36}$	$63.56^{\pm3.08}$	66.12	73.64
A-GEM	56.33 ^{±7.77}	$68.19^{\pm3.24}$	$25.21^{\pm 4.00}$	$43.83^{\pm0.69}$	$21.99^{\pm 4.01}$	$35.97^{\pm1.15}$	$30.53^{\pm 3.99}$	$49.26^{\pm0.64}$	$21.90^{\pm 5.52}$	$39.58^{\pm3.32}$	31.19	47.37
EEIL	82.34 ^{±3.13}	$90.50^{\pm0.72}$	$68.08^{\pm0.51}$			$79.54^{\pm0.69}$				$66.54^{\pm0.61}$	63.59	76.86
GD	89.16 ^{±0.53}		$64.36^{\pm0.57}$	$80.51^{\pm0.57}$		$78.43^{\pm0.76}$	$53.01^{\pm0.97}$			$63.91^{\pm0.40}$	61.82	76.92
DER++	84.63 ^{±2.91}		$69.73^{\pm0.99}$	$80.64^{\pm2.74}$	$70.03^{\pm 1.46}$	$81.72^{\pm 1.76}$	$55.84^{\pm 2.21}$	$66.55^{\pm3.73}$	$54.20^{\pm3.28}$	$67.14^{\pm 1.40}$	66.89	77.01
HAL	84.38 ^{±2.70}		$67.17^{\pm 1.50}$			$77.85^{\pm1.71}$		$65.31^{\pm3.68}$			65.39	74.41
DER	86.79 ^{±1.20}	$92.83^{\pm1.10}$	$73.30^{\pm0.58}$	$82.89^{\pm0.45}$	$72.00^{\pm0.57}$	$82.79^{\pm0.76}$	$59.57^{\pm0.89}$	$70.32^{\pm0.57}$	$57.18^{\pm 1.40}$	$70.21^{\pm0.86}$	69.77	79.81
FOSTER	86.09 ^{±0.38}	$91.54^{\pm0.65}$	$71.69^{\pm0.24}$	$81.16^{\pm0.39}$	$72.91^{\pm0.45}$	$83.02^{\pm0.86}$	$54.44^{\pm0.28}$	$69.95^{\pm0.28}$	$55.70^{\pm0.40}$	$70.00^{\pm0.26}$	68.17	79.13
BEEF	87.10 ^{±1.38}	$93.10^{\pm1.21}$	$72.09^{\pm0.33}$	$81.91^{\pm0.58}$		$81.45^{\pm0.74}$		$71.21^{\pm0.57}$	$58.16^{\pm0.60}$	$71.16^{\pm0.82}$	70.13	79.77
MORE	89.16 ^{±0.96}		$70.23^{\pm 2.27}$	$81.24^{\pm1.24}$			$64.97^{\pm 1.28}$	$74.03^{\pm 1.61}$	$63.06^{\pm1.26}$	$72.74^{\pm1.04}$	71.59	80.77
ROW	90.97 ^{±0.19}	$94.45^{\pm0.21}$	$74.72^{\pm0.48}$	$82.87^{\pm0.41}$	$74.60^{\pm0.12}$	$83.12^{\pm0.23}$	$65.11^{\pm 1.97}$	$74.16^{\pm1.34}$	$63.21^{\pm 2.53}$	$72.91^{\pm 2.12}$	73.72	81.50
TPLR	92.33 ^{±0.32}	95.11 ^{±0.44}	76.53 ^{±0.27}	$84.10^{\pm0.34}$	76.34 ^{±0.38}	84.46 ^{±0.28}	$68.64^{\pm0.44}$	76.77 ^{±0.23}	67.20 ^{±0.51}	$75.72^{\pm0.37}$	76.21	83.23

For TinyImageNet, we split 200 classes into 5 tasks (40 classes per task) (**T-5T**) and 10 tasks (20 classes per task) (**T-10T**). We set the replay buffer size for CIFAR-10 as 200 samples, and CIFAR-100 and TinyImageNet as 2000 samples following Kim et al. (2023). Following the random class order protocol in Rebuffi et al. (2017), we randomly generate five different class orders for each experiment and report the averaged metrics over the 5 random orders. For a fair comparison, the class orderings are kept the same for all systems. Results on a larger dataset are given in Appendix B.2.

Backbone Architectures. We conducted two sets of experiments, one using a pre-trained model and one without using a pre-trained model. Here we focus on using a pre-trained model as that is getting more popular. Following the TIL+OOD works (Kim et al., 2022a; 2023), which are our direct competitors, we use the same DeiT-S/16 model (Touvron et al., 2021) that was pre-trained using 611 classes of ImageNet after removing 389 classes that are similar or identical to the classes of the experiment data CIFAR and TinyImageNet to prevent information leak (Kim et al., 2022a; 2023). To leverage the pre-trained model while adapting to new knowledge, We insert an adapter module (Houlsby et al., 2019) at each transformer layer except SLDA and L2P.⁶ The adapter modules, classifiers and the layer norms are trained using HAT while the transformer parameters are fixed to prevent CF. The hidden dimension of adapters is 64 for CIFAR-10, and 128 for CIFAR-100 and TinyImageNet. The results without using a pre-trained model are given in Appendix B.3.

Evaluation Metrics. We follow Kim et al. (2022a) to use three metrics: (1) accuracy after learning the final task (**Last** in Table 1), (2) average incremental accuracy (**Avg** in Table 1), and (3) forgetting rate (see Figure 3). The definition of these metrics are given in Appendix B.1.

5.2 RESULTS AND COMPARISONS

Table 1 shows the CIL accuracy (ACC) results. Our TPLR performs the best consistently in each experiment with the average ACC (Last) of 76.21% while the best baseline ROW achieves 73.72%.

Comparison with CIL baselines with pre-training. The best-performing replay-based baseline is ROW, which also follows the TIL+OOD paradigm (Kim et al., 2022b) and ROW directly adopts the OOD score $S_{MD}(\boldsymbol{x})$. Since the score is inferior to our principled $S_{LR}(\boldsymbol{x})$, ROW is greatly outperformed by TPLR. The performance gap between our TPLR and the exemplar-free methods is even greater. The best non-replay based method PASS achieves Last ACC of 68.25%, which is outperformed by TPLR (76.21%) with a large margin. Another line of strong baselines are based on *network expansion*, including DER, FOSTER, and BEEF. They are also outperformed by TPLR on each dataset, indicating that the better task-id prediction is crucial in CIL. We report **ablation results** in the next section.

Without pre-training. The accuracy after learning the final task without pre-training are given in Table 5 of Appendix B.3. We provide a summary in Table 2 here. As L2P, SLDA, and ADAM

⁶SLDA fine-tunes only the classifier with a fixed feature extractor and L2P trains learnable prompts.

Table 2: CIL ACC (%) after learning the final task without pre-training (average over the five datasets used in Table 1). The detailed results are shown in Table 5 of Appendix B.3.

OWM	PASS	EEIL	GD	HAL	A-GEM	HAT	iCaRL
24.7	30.6	46.3	47.1	46.4	45.8	39.5	45.6
DER++	DER	FOSTER	BEEF	MORE	ROW	TPLF	R (ours)
46.5	54.2	52.2	53.4	51.2	53.1	5	7.5

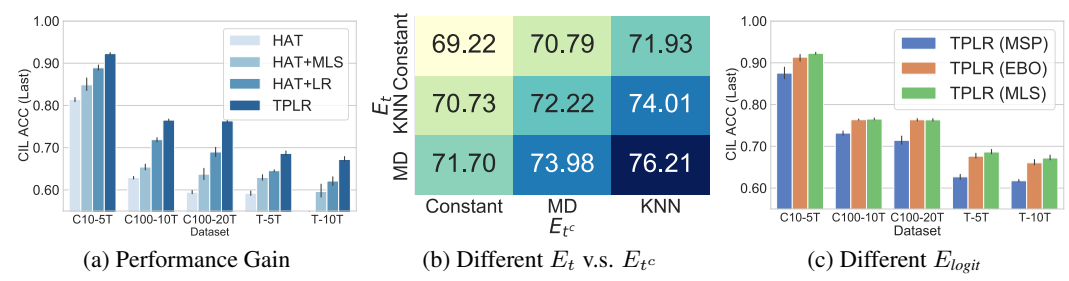


Figure 2: Ablation Studies. Fig (a) illustrates the achieved ACC gain for each of the designed techniques on the five datasets; Fig (b) displays the average ACC results obtained from different choices of E_t and E_{t^c} for eq. (7); Fig (c) showcases the results for various selections of E_{logit} for TPLR in eq. (9).

are designed specifically for pre-trained backbones, they cannot be adapted to the non-pre-training setting and thus are excluded here. Similar to the observation in Table 1, our TPLR achieves the overall best results (with ACC of 57.5%), while DER ranks the second (54.2%).

5.3 ABLATION STUDY

Performance Gain. Figure 2(a) shows the performance gain achieved by adding each proposed technique. Starting from vanilla HAT with an average Last ACC of 63.41% over all datasets, the proposed likelihood ratio LR score (HAT+LR) boosts the average Last ACC to 71.25%. Utilizing the OOD detection method MLS (HAT+MLS) only improves the ACC to 68.69%. The final composition of LR and MLS boosted the performance to 76.21%.

Different E_t v.s. E_{t^c} . Recall that the key insight behind the LR score lies in the estimation of likelihood ratio. Figure 2(b) presents the average Last ACC results across 5 datasets, employing various approaches to estimate \mathcal{P}_t and \mathcal{P}_{t^c} . In this context, the term *Constant* refers to the use of a uniform distribution as the distribution of \mathcal{P}_{t^c} , where the energy function is a constant mapping. Our TPLR approach is equivalent to employing ($E_t = \text{MD}$, $E_{t^c} = \text{KNN}$). The results reveal the following: (1) The incorporation of the \mathcal{P}_{t^c} distribution estimation is beneficial compared to assuming a uniform distribution. (2) As \mathcal{P}_{t^c} can only be estimated using the replay data, the high-performing KNN method outperforms MD. However, since MD can estimate \mathcal{P}_t without task t's training data during the test phase, it proves to be more effective than KNN when serving as E_t .

Different Logit-based Scores. Although $S_{MLS}(x)$ is used as the logit-based score in Section 4.2.2, alternative logit-based scores can also be considered. In this study, we conduct experiments using 3 popular logit-based scores MSP (Hendrycks & Gimpel, 2016), EBO (Liu et al., 2020a), and MLS (their definitions are given in Appendix D.2). The results presented in Figure 2(c) indicate that EBO and MLS yield comparable results, with average Last ACC of 75.76%, and 76.21% respectively, while MSP has inferior performance with average Last ACC of 71.32%.

Smaller Replay Buffer Sizes. The accuracy after learning the final task with smaller replay buffer sizes are given in Table 6 of Appendix B.4. We provide a summary as Table 3, which shows that when using a smaller replay buffer, the performance drop of TPLR is small. The goal of using the replay data in TPLR is to compute the likelihood ratio (LR) score, while traditional replay methods focus on preventing forgetting (CF). Note that CF is already addressed by the

Table 3: ACC (%) after learning the final task (Last) with smaller replay buffer sizes (average over the five datasets in Table 1). The detailed results are shown in Table 6 of Appendix B.4. The replay buffer size is set as 100 for CIFAR-10, and 1000 for CIFAR-100 and TinyImageNet.

iCaRL	A-GEM	EEIL	GD	DER++	HAL
63.60	31.15	58.24	54.39	62.16	60.21
DER	FOSTER	BEEF	MORE	ROW	TPLR
68.32	66.86	68.94	71.44	72.70	75.56

TIL method HAT in our case. Thus our method TPLR is robust with fewer replay samples.

Choices of β_1 and β_2 . β_1 and β_2 are two scaling hyper-parameters used in the definition of task-id prediction score $S_{TPLR}^{(t)}(x)$. Table 7 in Appendix B.5 shows an ablation for different β_1 and β_2 on C10-5T, which indicates that β_1 and β_2 do not affect results much. For other hyper-parameters used in TPLR, see Appendix F.1 for more details.

6 CONCLUSION

In this paper, we developed a novel approach for class incremental learning (CIL) via task-id prediction based on likelihood ratio. Recent studies (Kim et al., 2022a;b; 2023) suggested that OOD detection methods can be applied to perform task-id prediction in CIL and thus achieve the *state-of-the-art* performance. However, we argue that traditional OOD detection is not optimal for CIL as additional information in CIL can be leveraged to design a better and principled method for task-id prediction. Our experimental results show that our TPLR outperforms strong baselines and establishes a new state-of-the-art. Limitations of our approach are discussed in Appendix G.

ETHICS STATEMENT

Since this research involves only classification learning using existing datasets downloaded from the public domain and our algorithms are not for any specific application but for solving the general problem of continual learning, we do not feel there are any possible ethical issues in this research.

REPRODUCIBILITY STATEMENT

Our code is publicly available at https://github.com/linhaowei1/TPLR. The proofs of Theorems 4.1 and 4.2 are provided in Appendix C. The training details and dataset details are given in Section 5.1 and Appendix F.

REFERENCES

Davide Abati, Jakub Tomczak, Tijmen Blankevoort, Simone Calderara, Rita Cucchiara, and Babak Ehteshami Bejnordi. Conditional channel gated networks for task-aware continual learning. In *Proceedings of the IEEE/CVF Conference on Computer Vision and Pattern Recognition*, pp. 3931–3940, 2020. 2, 3

Rahaf Aljundi, Punarjay Chakravarty, and Tinne Tuytelaars. Expert gate: Lifelong learning with a network of experts. In *Proceedings of the IEEE Conference on Computer Vision and Pattern Recognition*, pp. 3366–3375, 2017. 3

Jihwan Bang, Hyunseo Koh, Seulki Park, Hwanjun Song, Jung-Woo Ha, and Jonghyun Choi. Online continual learning on a contaminated data stream with blurry task boundaries. In *Proceedings of the IEEE/CVF Conference on Computer Vision and Pattern Recognition*, pp. 9275–9284, 2022. 27

Magdalena Biesialska, Katarzyna Biesialska, and Marta R Costa-Jussa. Continual lifelong learning in natural language processing: A survey. *arXiv preprint arXiv:2012.09823*, 2020. 3

Pietro Buzzega, Matteo Boschini, Angelo Porrello, Davide Abati, and Simone Calderara. Dark experience for general continual learning: a strong, simple baseline. *Advances in neural information processing systems*, 33:15920–15930, 2020. 7

Francisco M Castro, Manuel J Marín-Jiménez, Nicolás Guil, Cordelia Schmid, and Karteek Alahari. End-to-end incremental learning. In *Proceedings of the European conference on computer vision (ECCV)*, pp. 233–248, 2018. 7

Arslan Chaudhry, Marc'Aurelio Ranzato, Marcus Rohrbach, and Mohamed Elhoseiny. Efficient lifelong learning with a-gem. *arXiv preprint arXiv:1812.00420*, 2018. 7

Arslan Chaudhry, Albert Gordo, Puneet Dokania, Philip Torr, and David Lopez-Paz. Using hindsight to anchor past knowledge in continual learning. In *Proceedings of the AAAI Conference on Artificial Intelligence*, volume 35, pp. 6993–7001, 2021. 7

- Peng Cui and Jinjia Wang. Out-of-distribution (ood) detection based on deep learning: A review. *Electronics*, 11(21):3500, 2022. 2
- Matthias De Lange, Rahaf Aljundi, Marc Masana, Sarah Parisot, Xu Jia, Aleš Leonardis, Gregory Slabaugh, and Tinne Tuytelaars. A continual learning survey: Defying forgetting in classification tasks. *IEEE transactions on pattern analysis and machine intelligence*, 44(7):3366–3385, 2021. 1, 3
- Yilun Du, Shuang Li, and Igor Mordatch. Compositional visual generation with energy based models. *Advances in Neural Information Processing Systems*, 33:6637–6647, 2020. 7
- Yiduo Guo, Bing Liu, and Dongyan Zhao. Online continual learning through mutual information maximization. In *International Conference on Machine Learning*, pp. 8109–8126. PMLR, 2022. 27
- Raia Hadsell, Dushyant Rao, Andrei A Rusu, and Razvan Pascanu. Embracing change: Continual learning in deep neural networks. *Trends in cognitive sciences*, 24(12):1028–1040, 2020. 3
- Tyler L Hayes and Christopher Kanan. Lifelong machine learning with deep streaming linear discriminant analysis. In *Proceedings of the IEEE/CVF conference on computer vision and pattern recognition workshops*, pp. 220–221, 2020. 7
- Kaiming He, Xiangyu Zhang, Shaoqing Ren, and Jian Sun. Deep residual learning for image recognition. In *Proceedings of the IEEE conference on computer vision and pattern recognition*, pp. 770–778, 2016. 18
- Dan Hendrycks and Kevin Gimpel. A baseline for detecting misclassified and out-of-distribution examples in neural networks. *arXiv preprint arXiv:1610.02136*, 2016. 2, 9
- Dan Hendrycks, Mantas Mazeika, and Thomas Dietterich. Deep anomaly detection with outlier exposure. *arXiv preprint arXiv:1812.04606*, 2018. 5
- Dan Hendrycks, Steven Basart, Mantas Mazeika, Mohammadreza Mostajabi, Jacob Steinhardt, and Dawn Song. Scaling out-of-distribution detection for real-world settings. arXiv preprint arXiv:1911.11132, 2019. 2
- Christian Henning, Maria Cervera, Francesco D'Angelo, Johannes Von Oswald, Regina Traber, Benjamin Ehret, Seijin Kobayashi, Benjamin F Grewe, and João Sacramento. Posterior meta-replay for continual learning. *Advances in Neural Information Processing Systems*, 34:14135–14149, 2021. 3
- Neil Houlsby, Andrei Giurgiu, Stanislaw Jastrzebski, Bruna Morrone, Quentin De Laroussilhe, Andrea Gesmundo, Mona Attariyan, and Sylvain Gelly. Parameter-efficient transfer learning for nlp. In *International Conference on Machine Learning*, pp. 2790–2799. PMLR, 2019. 4, 8
- Zixuan Ke, Bing Liu, Nianzu Ma, Hu Xu, and Lei Shu. Achieving forgetting prevention and knowledge transfer in continual learning. *Advances in Neural Information Processing Systems*, 34: 22443–22456, 2021a. 3
- Zixuan Ke, Hu Xu, and Bing Liu. Adapting bert for continual learning of a sequence of aspect sentiment classification tasks. In *Proceedings of the 2021 Conference of the North American Chapter of the Association for Computational Linguistics: Human Language Technologies*, pp. 4746–4755, 2021b. 3
- Zixuan Ke, Haowei Lin, Yijia Shao, Hu Xu, Lei Shu, and Bing Liu. Continual training of language models for few-shot learning. In *Empirical Methods in Natural Language Processing (EMNLP)*, 2022. 3
- Ronald Kemker and Christopher Kanan. Fearnet: Brain-inspired model for incremental learning. *arXiv preprint arXiv:1711.10563*, 2017. 1, 3
- Gyuhak Kim, Bing Liu, and Zixuan Ke. A multi-head model for continual learning via out-of-distribution replay. In *Conference on Lifelong Learning Agents*, pp. 548–563. PMLR, 2022a. 3, 7, 8, 10, 16, 17, 25

- Gyuhak Kim, Changnan Xiao, Tatsuya Konishi, Zixuan Ke, and Bing Liu. A theoretical study on solving continual learning. In *Advances in Neural Information Processing Systems*, 2022b. 1, 2, 3, 7, 8, 10, 16, 18
- Gyuhak Kim, Changnan Xiao, Tatsuya Konishi, and Bing Liu. Learnability and algorithm for continual learning. *arXiv preprint arXiv:2306.12646*, 2023. 2, 3, 7, 8, 10, 25
- Alex Krizhevsky and Geoff Hinton. Convolutional deep belief networks on cifar-10. *Unpublished manuscript*, 40(7):1–9, 2010. 25
- Alex Krizhevsky, Geoffrey Hinton, et al. Learning multiple layers of features from tiny images. 2009.
- Ya Le and Xuan Yang. Tiny imagenet visual recognition challenge. CS 231N, 7:7, 2015. 25
- Kibok Lee, Kimin Lee, Jinwoo Shin, and Honglak Lee. Overcoming catastrophic forgetting with unlabeled data in the wild. In *Proceedings of the IEEE/CVF International Conference on Computer Vision*, pp. 312–321, 2019. 7
- Kimin Lee, Honglak Lee, Kibok Lee, and Jinwoo Shin. Training confidence-calibrated classifiers for detecting out-of-distribution samples. In *International Conference on Learning Representations*, 2018a. 2
- Kimin Lee, Kibok Lee, Honglak Lee, and Jinwoo Shin. A simple unified framework for detecting out-of-distribution samples and adversarial attacks. *Advances in neural information processing systems*, 31, 2018b. 2, 6, 22
- Guodun Li, Yuchen Zhai, Qianglong Chen, Xing Gao, Ji Zhang, and Yin Zhang. Continual few-shot intent detection. In *Proceedings of the 29th International Conference on Computational Linguistics*, pp. 333–343, 2022. 3
- Shiyu Liang, Yixuan Li, and Rayadurgam Srikant. Enhancing the reliability of out-of-distribution image detection in neural networks. *arXiv preprint arXiv:1706.02690*, 2017. 2
- Weitang Liu, Xiaoyun Wang, John Owens, and Yixuan Li. Energy-based out-of-distribution detection. Advances in Neural Information Processing Systems, 33:21464–21475, 2020a. 2, 9
- Y. Liu, A. A. Liu, Y. Su, B. Schiele, and Q. Sun. Mnemonics training: Multi-class incremental learning without forgetting. In 2020 IEEE/CVF Conference on Computer Vision and Pattern Recognition (CVPR), 2020b. 17
- David Lopez-Paz and Marc'Aurelio Ranzato. Gradient episodic memory for continual learning. *Advances in neural information processing systems*, 30, 2017. 1, 3, 17
- Arun Mallya and Svetlana Lazebnik. Packnet: Adding multiple tasks to a single network by iterative pruning. In *Proceedings of the IEEE conference on Computer Vision and Pattern Recognition*, pp. 7765–7773, 2018. 3
- Michael McCloskey and Neal J Cohen. Catastrophic interference in connectionist networks: The sequential learning problem. In *Psychology of learning and motivation*, volume 24, pp. 109–165. Elsevier, 1989. 1
- Eric Nalisnick, Akihiro Matsukawa, Yee Whye Teh, Dilan Gorur, and Balaji Lakshminarayanan. Do deep generative models know what they don't know? *arXiv preprint arXiv:1810.09136*, 2018. 5
- Jerzy Neyman and Egon Sharpe Pearson. Ix. on the problem of the most efficient tests of statistical hypotheses. *Philosophical Transactions of the Royal Society of London. Series A, Containing Papers of a Mathematical or Physical Character*, 231(694-706):289–337, 1933. 5, 20
- Jathushan Rajasegaran, Salman Khan, Munawar Hayat, Fahad Shahbaz Khan, and Mubarak Shah. itaml: An incremental task-agnostic meta-learning approach. In *Proceedings of the IEEE/CVF Conference on Computer Vision and Pattern Recognition*, pp. 13588–13597, 2020. 2, 3

- Sylvestre-Alvise Rebuffi, Alexander Kolesnikov, Georg Sperl, and Christoph H Lampert. icarl: Incremental classifier and representation learning. In *Proceedings of the IEEE conference on Computer Vision and Pattern Recognition*, pp. 2001–2010, 2017. 1, 7, 8
- Olga Russakovsky, Jia Deng, Hao Su, Jonathan Krause, Sanjeev Satheesh, Sean Ma, Zhiheng Huang, Andrej Karpathy, Aditya Khosla, Michael Bernstein, Alexander C. Berg, and Li Fei-Fei. ImageNet Large Scale Visual Recognition Challenge. *International Journal of Computer Vision (IJCV)*, 115 (3):211–252, 2015. doi: 10.1007/s11263-015-0816-y. 17
- Joan Serra, Didac Suris, Marius Miron, and Alexandros Karatzoglou. Overcoming catastrophic forgetting with hard attention to the task. In *International Conference on Machine Learning*, pp. 4548–4557. PMLR, 2018. 2, 3, 4, 7, 24, 25
- Yiyou Sun, Chuan Guo, and Yixuan Li. React: Out-of-distribution detection with rectified activations. Advances in Neural Information Processing Systems, 34:144–157, 2021. 2
- Yiyou Sun, Yifei Ming, Xiaojin Zhu, and Yixuan Li. Out-of-distribution detection with deep nearest neighbors. *arXiv preprint arXiv:2204.06507*, 2022. 2, 6
- Jihoon Tack, Sangwoo Mo, Jongheon Jeong, and Jinwoo Shin. Csi: Novelty detection via contrastive learning on distributionally shifted instances. *Advances in neural information processing systems*, 33:11839–11852, 2020. 2, 3
- Hugo Touvron, Matthieu Cord, Matthijs Douze, Francisco Massa, Alexandre Sablayrolles, and Hervé Jégou. Training data-efficient image transformers & distillation through attention. In *International Conference on Machine Learning*, pp. 10347–10357. PMLR, 2021. 8
- S Vaze, K Han, A Vedaldi, and A Zisserman. Open-set recognition: A good closed-set classifier is all you need? In *International Conference on Learning Representations (ICLR)*, 2022. 2
- Johannes Von Oswald, Christian Henning, Benjamin F Grewe, and João Sacramento. Continual learning with hypernetworks. *arXiv preprint arXiv:1906.00695*, 2019. 2, 3
- Fu-Yun Wang, Da-Wei Zhou, Liu Liu, Han-Jia Ye, Yatao Bian, De-Chuan Zhan, and Peilin Zhao. Beef: Bi-compatible class-incremental learning via energy-based expansion and fusion. In *The Eleventh International Conference on Learning Representations*, 2022a. 3, 7
- Fu-Yun Wang, Da-Wei Zhou, Han-Jia Ye, and De-Chuan Zhan. Foster: Feature boosting and compression for class-incremental learning. In *European conference on computer vision*, pp. 398–414. Springer, 2022b. 7
- Haoqi Wang, Zhizhong Li, Litong Feng, and Wayne Zhang. Vim: Out-of-distribution with virtual-logit matching. In *Proceedings of the IEEE/CVF Conference on Computer Vision and Pattern Recognition*, pp. 4921–4930, 2022c. 6
- Liyuan Wang, Xingxing Zhang, Hang Su, and Jun Zhu. A comprehensive survey of continual learning: Theory, method and application, 2023. 1
- Mengyu Wang, Yijia Shao, Haowei Lin, Wenpeng Hu, and Bing Liu. Cmg: A class-mixed generation approach to out-of-distribution detection. *Proceedings of ECML/PKDD-2022*, 2022d. 2
- Zifeng Wang, Zizhao Zhang, Chen-Yu Lee, Han Zhang, Ruoxi Sun, Xiaoqi Ren, Guolong Su, Vincent Perot, Jennifer Dy, and Tomas Pfister. Learning to prompt for continual learning. In *Proceedings of the IEEE/CVF Conference on Computer Vision and Pattern Recognition*, pp. 139–149, 2022e. 3, 7
- Mitchell Wortsman, Vivek Ramanujan, Rosanne Liu, Aniruddha Kembhavi, Mohammad Rastegari, Jason Yosinski, and Ali Farhadi. Supermasks in superposition. *Advances in Neural Information Processing Systems*, 33:15173–15184, 2020. 3
- Shipeng Yan, Jiangwei Xie, and Xuming He. Der: Dynamically expandable representation for class incremental learning. In *Proceedings of the IEEE/CVF Conference on Computer Vision and Pattern Recognition*, pp. 3014–3023, 2021. 3, 7

- Jingkang Yang, Kaiyang Zhou, Yixuan Li, and Ziwei Liu. Generalized out-of-distribution detection: A survey. *arXiv preprint arXiv:2110.11334*, 2021. 2
- Jingkang Yang, Pengyun Wang, Dejian Zou, Zitang Zhou, Kunyuan Ding, Wenxuan Peng, Haoqi Wang, Guangyao Chen, Bo Li, Yiyou Sun, Xuefeng Du, Kaiyang Zhou, Wayne Zhang, Dan Hendrycks, Yixuan Li, and Ziwei Liu. Openood: Benchmarking generalized out-of-distribution detection. 2022. 6
- Guanxiong Zeng, Yang Chen, Bo Cui, and Shan Yu. Continual learning of context-dependent processing in neural networks. *Nature Machine Intelligence*, 1(8):364–372, 2019. 3, 7
- Da-Wei Zhou, Han-Jia Ye, De-Chuan Zhan, and Ziwei Liu. Revisiting class-incremental learning with pre-trained models: Generalizability and adaptivity are all you need. *arXiv preprint arXiv:2303.07338*, 2023. 7
- Fei Zhu, Xu-Yao Zhang, Chuang Wang, Fei Yin, and Cheng-Lin Liu. Prototype augmentation and self-supervision for incremental learning. In *Proceedings of the IEEE/CVF Conference on Computer Vision and Pattern Recognition*, pp. 5871–5880, 2021. 3, 7

Appendix of TPLR

Table of Contents

A	Output Calibration	16
В	Extra Experimental Results	17
	B.1 Forgetting Rate Experiment Results and Definitions of Accuracy Metrics	17
	B.2 CIL Experiments on a Larger Dataset	17
	B.3 CIL Experiments without Pre-training	18
	B.4 CIL Experiments on Smaller Replay Buffer Size	19
	B.5 Ablation on β_1 and β_2	19
C	Theoretical Justifications	20
	C.1 Preliminary	20
	C.2 Proof of Theorem 4.1	20
	C.3 Proof of Theorem 4.2	20
	C.4 Distance-Based OOD Detectors are IND Density Estimators	21
D	Additional Details about TPLR	22
	D.1 Computation of the MD Score	22
	D.2 Computation of Logit-based Scores	22
	D.3 Pseudo-code	22
E	Details of HAT	24
F	Implementation Details, Network Size and Running Time	25
	F.1 Implementation Details of Baselines	25
	F.2 Hardware and Software	25
	F.3 Computational Budget Analysis	25
G	Limitations	27

A OUTPUT CALIBRATION

We used the output calibration technique to balance the scales of task-id prediction scores for different tasks, which is motivated by Kim et al. (2022a;b). Even if the task-id prediction of each task-model is perfect, the system can make an incorrect task-id prediction if the magnitudes of the outputs across different tasks are different. As the task-specific modules are trained separately in HAT, it is useful to calibrate the outputs of different task modules.

To ensure that the output values are comparable, we calibrate the outputs by scaling $\sigma_1^{(t)}$ and shifting $\sigma_2^{(t)}$ parameters for each task. The optimal parameters $\{(\sigma_1^{(t)},\sigma_2^{(t)})\}_{t=1}^T \in \mathbb{R}^{2T}$ (T is the number of tasks) can be found by solving optimization problem using samples in the replay buffer Buf .

Specifically, we minimize the cross-entropy loss using SGD optimizer with batch size 64 for 100 epochs to find optimal calibration parameters $\{(\sigma_1^{(t)}, \sigma_2^{(t)})\}_{t=1}^T$:

$$\mathcal{L}_{calibration} = -\mathbb{E}_{(\boldsymbol{x},y) \in Buf} \log p(y|\boldsymbol{x}),$$

where p(y|x) is computed using eq. (3) and calibration parameters:

$$p(y_j^{(t)}|\boldsymbol{x}) = \sigma_1^{(t)} \cdot \left[\textit{softmax}\left(f(h(\boldsymbol{x}; \phi^{(t)}); \theta^{(t)}) \right) \right]_j \cdot S(\boldsymbol{x}; t) + \sigma_2^{(t)}$$

Given the optimal parameters $\{(\tilde{\sigma}_1^{(t)}, \tilde{\sigma}_2^{(t)})\}_{t=1}^T$, we make the final prediction as:

$$\hat{y} = \underset{1 \le t \le T, 1 \le j \le |\mathcal{Y}_t|}{\arg \max} p(y_j^{(t)} | \boldsymbol{x})$$

B EXTRA EXPERIMENTAL RESULTS

B.1 FORGETTING RATE EXPERIMENT RESULTS AND DEFINITIONS OF ACCURACY METRICS



Figure 3: Average forgetting rate (%) on C10-5T, C100-10T, and C100-20T. The lower the rate, the better the method is. The methods in the figures are sorted in descending order of the average forgetting rate.

Apart from the *classification accuracy* (ACC), we report another popular CIL evaluation metric average forgetting rate (Liu et al., 2020b) of CIL baselines and our system TPLR in this section as a complement to Table 1. The average forgetting rate after task t is defined as

$$\mathcal{F}^{(t)} = \frac{1}{t-1} \sum_{i=1}^{t-1} (A_i^{(i)} - A_i^{(t)}),$$

where $A_i^{(t)}$ is the accuracy of the model on task *i*-th test set after learning task *t*. The average forgetting rate is also referred as *backward transfer* in other literature (Lopez-Paz & Ranzato, 2017).

It is useful to note that our TPLR's forgetting has been handled by the masking mechanism in the TIL method HAT. Here the forgetting rate mainly reflect how the number of tasks affect the results of TPLR.

Figure 3 shows the average forgetting rate of each baseline after learning the last task. The forgetting rates of our proposed TPLR are 4.33%, 8.08%, and 8.16% on C10-5T, C100-10T and C100-20T, respectively. Our TPLR has the lowest forgetting rate on the three datasets compared to the 17 baselines. iCaRL has the lowest forgetting rate on average among the 17 baselines. We also note that iCaRL's Last ACC values are much lower than TPLR on the same experiments: The average Last ACC of TPLR is 76.21% while that of iCaRL is only 66.12%. In a sharp contrast, the best baseline ROW (with the highest average Last ACC of 73.72%) among all the baselines adapts to new knowledge effectively, but it was not able to retain the knowledge as well as our method. Its forgetting rates are 7.55%, 8.83%, and 9.92% on C10-5T, C100-10T, and C100-20T, respectively, which are larger than ours.

Definitions of Avg. and Last accuracy: Fllowing (Kim et al., 2022a), we give the formal definitions of average incremental accuracy (**Avg** in Table 1 in the main text, denoted as A_{avg}) and accuracy after learning the final task (**Last** in Table 1 in the main text, denoted as A_{last}). Let the accuracy after learning the task t be:

$$A^{(\leq t)} = \frac{\# correctly \ classified \ samples \ in \ \bigcup_{k=1}^{t} \mathcal{D}^{(k)}_{test}}{\# samples \ in \ \bigcup_{k=1}^{t} \mathcal{D}^{(k)}_{test}}$$

Let T be the last task. Then, $A_{last} = A^{(\leq T)}$ and $A_{avg} = \frac{1}{T} \sum_{k=1}^{T} A^{(\leq k)}$.

Here $\mathcal{D}^{(k)}_{\textit{test}}$ denotes the test-set for task k, and # denotes "the number of". To put it simply, $A^{(\leq t)}$ means the accuracy of all the test data from task t.

B.2 CIL EXPERIMENTS ON A LARGER DATASET

To assess the performance of our proposed TPLR on large-scale datasets, we use ImageNet-1k (Russakovsky et al., 2015), a widely recognized benchmark dataset frequently examined in the CIL

Table 4: The CIL ACC after the final task on ImageNet380-10T. We highlight the best results in bold.

HAT	ADAM	SLDA	PASS	L2P	iCaRL	A-GEM	EEIL
$71.20^{\pm0.99}$	$62.10^{\pm0.91}$	$65.78^{\pm0.05}$	$65.27^{\pm1.24}$	$47.89^{\pm3.24}$	$62.23^{\pm0.66}$	$30.38^{\pm10.02}$	$63.37^{\pm0.49}$
DER++	HAL	DER	FORSTER	BEEF	MORE	ROW	TPLR

literature. However, due to the nature of our experiments, which involve a DeiT backbone pretrained on 611 ImageNet classes after excluding 389 classes similar to those in CIFAR and TinyImageNet, we cannot directly evaluate our model on the original ImageNet dataset to avoid potential information leak.

To overcome this limitation, we created a new benchmark dataset called **ImageNet-380**. We randomly selected 380 classes from the remaining 389 classes, excluding those similar to CIFAR and TinyImageNet, from the original set of 1k classes in the full ImageNet dataset. This new dataset consists of approximately 1,300 color images per class. For ImageNet-380, we divided the classes into 10 tasks, with each task comprising 38 classes. We set the replay buffer size to 7600, with 20 samples per class, which is a commonly used number in replay-based methods. We refer to these experiments as ImageNet380-10T. For other training configurations, we kept them consistent with the experiments conducted on T-10T.

The CIL Last ACC achieved after the final task on ImageNet380-10T can be found in Table 4. Notably, the results obtained by \mathtt{TPLR} still exhibit a significant improvement over the baselines, with a 3.97% higher ACC compared to the best baseline method \mathtt{ROW} . The results further provide strong evidence supporting the effectiveness of our proposed \mathtt{TPLR} system.

B.3 CIL Experiments without Pre-training

Table 5: CIL accuracy (%) after the final task (last) based on ResNet-18 without pre-training over 5 runs with random seeds. "-XT": X number of tasks. The best result in each column is highlighted in bold.

	C10-5T	C100-10T	C100-20T	T-5T	T-10T	Average
OWM	$51.8^{\pm0.05}$	$28.9^{\pm0.60}$	$24.1^{\pm0.26}$	$10.0^{\pm0.55}$	$8.6^{\pm0.42}$	24.7
PASS	$47.3^{\pm0.98}$	$33.0^{\pm0.58}$	$25.0^{\pm0.69}$	$28.4^{\pm0.51}$	$19.1^{\pm0.46}$	30.6
EEIL	$64.5^{\pm0.93}$	$52.3^{\pm0.83}$	$48.0^{\pm0.44}$	$38.2^{\pm0.54}$	$28.7^{\pm0.87}$	46.3
GD	$65.5^{\pm0.94}$	$51.4^{\pm0.83}$	$50.3^{\pm0.88}$	$38.9^{\pm 1.01}$	$29.5^{\pm0.68}$	47.1
HAL	$63.7^{\pm0.91}$	$51.3^{\pm 1.22}$	$48.5^{\pm0.71}$	$38.1^{\pm0.97}$	$30.3^{\pm 1.05}$	46.4
A-GEM	$64.6^{\pm0.72}$	$50.5^{\pm0.73}$	$47.3^{\pm0.87}$	$37.3^{\pm0.89}$	$29.4^{\pm0.95}$	45.8
HAT	$62.7^{\pm 1.45}$	$41.1^{\pm0.93}$	$25.6^{\pm0.51}$	$38.5^{\pm 1.85}$	$29.8^{\pm0.65}$	39.5
iCaRL	$63.4^{\pm 1.11}$	$51.4^{\pm0.99}$	$47.8^{\pm0.48}$	$37.0^{\pm0.41}$	$28.3^{\pm0.18}$	45.6
DER++	$66.0^{\pm 1.20}$	$53.7^{\pm 1.20}$	$46.6^{\pm 1.44}$	$35.8^{\pm0.77}$	$30.5^{\pm0.47}$	46.5
DER	$62.1^{\pm0.97}$	$64.5^{\pm0.85}$	$62.5^{\pm0.76}$	$43.6^{\pm0.77}$	$38.3^{\pm0.82}$	54.2
FOSTER	$65.4^{\pm 1.05}$	$62.5^{\pm0.84}$	$56.3^{\pm0.71}$	$40.5^{\pm0.92}$	$36.4^{\pm0.85}$	52.2
BEEF	$67.3^{\pm 1.07}$	$60.9^{\pm0.87}$	$56.7^{\pm0.72}$	$44.1^{\pm0.85}$	$37.9^{\pm0.95}$	53.4
MORE	$70.6^{\pm0.74}$	$57.5^{\pm0.68}$	$51.3^{\pm0.89}$	$41.2^{\pm0.81}$	$35.4^{\pm0.72}$	51.2
ROW	$74.6^{\pm0.89}$	$58.2^{\pm0.67}$	$52.1^{\pm0.91}$	$42.3^{\pm0.69}$	$38.2^{\pm 1.34}$	53.1
TPLR	78.4 ^{±0.78}	$62.2^{\pm0.52}$	$55.8^{\pm0.57}$	48.2 ^{±0.64}	42.9 ^{±0.45}	57.5

The experimental setup and results for CIL baselines without pre-training are presented in this section.

Training details. We follow Kim et al. (2022b) to use ResNet-18 (He et al., 2016) for all the datasets (CIFAR-10, CIFAR-100, TinyImageNet) and all the baselines excluding OWM. MORE, ROW, and our TPLR are designed for pre-trained models, and we adapt them by applying HAT on ResNet-18. All other baselines adopted ResNet-18 in their original paper. OWM adopts AlexNet as it is hard to apply the method to the ResNet. For the replay-based methods, we also use the same buffer size as specified in Section 5.1. We use the hyper-parameters suggested by their original papers. For MORE, ROW, and our proposed TPLR, we follow the hyper-parameters used in HAT for training.

Experimental Results. The results for CIL Last accuracy (ACC) after the final task are shown in Table 5. We can observe that the network-expansion-based approaches (DER, FOSTER, BEEF) and approaches that predict task-id based on TIL+OOD (MORE, ROW) are two competitive groups of CIL baselines. Our proposed TPLR achieves the best performance on C10-5T, T-5T, and T-10T, while DER achieves the best on C100-10T and C100-20T. Overall, our proposed TPLR achieves the best average accuracy over the 5 datasets (57.5%) while DER ranks the second (with an average ACC of 54.2%).

B.4 CIL EXPERIMENTS ON SMALLER REPLAY BUFFER SIZE

Table 6: CIL accuracy (%) after the final task (Last) with smaller replay buffer size over 5 runs with random seeds. "-XT": X number of tasks. The best result in each column is highlighted in bold. The replay buffer size is set to 100 for CIFAR-10, and 1000 for CIFAR-100 and TinyImageNet. The pre-trained model is used

	C10-5T	C100-10T	C100-20T	T-5T	T-10T	Average
iCaRL	86.08 ^{±1.19}	$66.96^{\pm 2.08}$	$68.16^{\pm0.71}$	$47.27^{\pm3.22}$	$49.51^{\pm1.87}$	63.60
A-GEM	56.64 ^{±4.29}	$23.18^{\pm 2.54}$	$20.76^{\pm 2.88}$	$31.44^{\pm3.84}$	$23.73^{\pm 6.27}$	31.15
EEIL	$77.44^{\pm 3.04}$	$62.95^{\pm0.68}$	$57.86^{\pm0.74}$	$48.36^{\pm1.38}$	$44.59^{\pm 1.72}$	58.24
GD	$85.96^{\pm 1.64}$	$57.17^{\pm 1.06}$	$50.30^{\pm0.58}$	$46.09^{\pm1.77}$	$32.41^{\pm 2.75}$	54.39
DER++	$80.09^{\pm 3.00}$	$64.89^{\pm 2.48}$	$65.84^{\pm1.46}$	$50.74^{\pm 2.41}$	$49.24^{\pm 5.01}$	62.16
HAL	$79.16^{\pm 4.56}$	$62.65^{\pm0.83}$	$63.96^{\pm1.49}$	$48.17^{\pm 2.94}$	$47.11^{\pm 6.00}$	60.21
DER	85.11 ^{±1.44}	$72.31^{\pm0.78}$	$70.25^{\pm0.98}$	$58.07^{\pm 1.40}$	$55.85^{\pm1.23}$	68.32
FOSTER	$84.99^{\pm0.89}$	$70.25^{\pm0.58}$	$71.14^{\pm0.76}$	$53.35^{\pm0.54}$	$54.58^{\pm0.85}$	66.86
BEEF	86.20 ^{±1.59}	$70.87^{\pm 2.77}$	$70.44^{\pm 1.24}$	$60.15^{\pm0.98}$	$57.02^{\pm0.87}$	68.94
MORE	88.13 ^{±1.16}	$71.69^{\pm0.11}$	$71.29^{\pm0.55}$	$64.17^{\pm0.77}$	$61.90^{\pm0.90}$	71.44
ROW	$89.70^{\pm1.54}$	$73.63^{\pm0.12}$	$71.86^{\pm0.07}$	$65.42^{\pm0.55}$	$62.87^{\pm0.53}$	72.70
TPLR	91.76 ^{±0.44}	75.83 $^{\pm0.28}$	75.65 ^{±0.54}	68.08 ^{±0.61}	66.48 ^{±0.47}	75.56

B.5 Ablation on β_1 and β_2

Table 7: The CIL accuracy (%) after leraning the final task (Last) of our TPLR on C10-5T for different β_1 and β_2 .

β_1 β_2	15.0	17.5	20.0	22.5	25.0
0.5	91.9	91.9	91.8	92.5	92.2
0.6	92.1	91.0	92.2	91.6	92.0
0.7	91.8	92.1	92.3	92.4	91.9
0.8	92.0	92.4	91.7	91.9	91.7
0.9	92.3	92.5	92.0	91.9	91.5

C THEORETICAL JUSTIFICATIONS

C.1 PRELIMINARY

In this section, we first give some primary definitions and notations of *statistical hypothesis testing*, rejection region and uniformly most powerful (UMP) test.

Definition 1 (statistical hypothesis testing and rejection region) Consider testing a null hypothesis $H_0: \theta \in \Theta_0$ against an alternative hypothesis $H_1: \theta \in \Theta_1$, where Θ_0 and Θ_1 are subsets of the parameter space Θ and $\Theta_0 \cap \Theta_1 = \emptyset$. A test consists of a test statistic T(X), which is a function of the data x, and a rejection region \mathcal{R} , which is a subset of the range of T. If the observed value t of T falls in \mathcal{R} , we reject H_0 .

Type I error occurs when we reject a true null hypothesis \mathcal{H}_0 . The probability of making Type I error is usually denoted by α . **Type II error** occurs when we *fail to reject* a false null hypothesis \mathcal{H}_0 . The **level of significance** α is the probability we are willing to risk rejecting \mathcal{H}_0 when it is true. Typically $\alpha = 0.1, 0.05, 0.01$ are used.

Definition 2 (UMP test) Denote the power function $\beta_{\mathcal{R}}(\theta) = P_{\theta}(T(x) \in \mathcal{R})$, where P_{θ} denotes the probability measure when θ is the true parameter. A test with a test statistic T and rejection region \mathcal{R} is called a **uniformly most powerful (UMP)** test at significance level α if it satisfies two conditions:

- 1. $\sup_{\theta \in \Theta_0} \beta_{\mathcal{R}}(\theta) \leq \alpha$.
- 2. $\forall \theta \in \Theta_1, \beta_{\mathcal{R}}(\theta) \geq \beta_{R'}(\theta)$ for every other test t' with rejection region R' satisfying the first condition.

From the definition we see, the UMP test ensures that the probability of Type I error is less than α (with the first condition), while achieves the lowest Type II error (with the second condition). Therefore, UMP is considered an optimal solution in statistical hypothesis testing.

C.2 PROOF OF THEOREM 4.1

Lemma C.1 (Neyman & Pearson, 1933) Let $\{X_1, X_2, ..., X_n\}$ be a random sample with likelihood function $L(\theta)$. The UMP test of the simple hypothesis $H_0: \theta = \theta_0$ against the simple hypothetis $H_a: \theta = \theta_a$ at level α has a rejection region of the form:

$$\frac{L(\theta_0)}{L(\theta_a)} < k$$

where k is chosen so that the probability of a type I error is α .

Now the proof of Theorem 4.1 is straightforward. From Lemma C.1, the UMP test for Equation (4) in the main text has a rejection region of the form:

$$rac{p_t(oldsymbol{x})}{p_{t^c}(oldsymbol{x})} < \lambda_0$$

where λ_0 is chosen so that the probability of a type I error is α .

C.3 Proof of Theorem 4.2

Note that the AUC is computed as the *area under the ROC curve*. A ROC curve shows the trade-off between true positive rate (TPR) and false positive rate (FPR) across different decision thresholds. Therefore,

$$AUC = \int_0^1 (TPR) \, \mathrm{d}(FPR) \tag{12}$$

$$= \int_{0}^{1} (1 - FPR) \, d(TPR) \tag{13}$$

$$= \int_0^1 \beta_{\mathcal{R}}(\theta_{t^c}) \, \mathrm{d}(1 - \beta_{\mathcal{R}}(\theta_t)) \tag{14}$$

$$= \int_0^1 \beta_{\mathcal{R}}(\theta_{t^c}) \, \mathrm{d}\beta_{\mathcal{R}}(\theta_t) \tag{15}$$

where FPR and TPR are false positive rate and true positive rate. Therefore, an optimal AUC requires UMP test of any given level $\alpha = \beta_{\mathcal{R}}(\theta_t)$ except on a null set.

C.4 DISTANCE-BASED OOD DETECTORS ARE IND DENSITY ESTIMATORS

In this section, we show that $S_{MD}(x)$ (MD: Mahalanobis distance) and $S_{KNN}(x)$ (KNN: k-nearest neighbor) defined in Equation (16) and Equation (17) are IND (in-distribution) density estimators under different assumptions (We omit the superscript (t) for simplicity):

$$S_{MD}(\boldsymbol{x}) = 1/\min_{c \in \mathcal{V}} (\boldsymbol{z} - \boldsymbol{\mu}_c)^T \boldsymbol{\Sigma}^{-1} (\boldsymbol{z} - \boldsymbol{\mu}_c), \tag{16}$$

$$S_{KNN}(\boldsymbol{x}; \mathcal{D}) = -||\boldsymbol{z}^* - kNN(\boldsymbol{z}^*; \mathcal{D}^*)||_2. \tag{17}$$

In Equation (16), μ_c is the class centroid for class c and Σ is the global covariance matrix, which are estimated on IND training corpus \mathcal{D} . In Equation (17), $||\cdot||_2$ is Euclidean norm, $z^* = z/||z||_2$ denotes the normalized feature z, and \mathcal{D}^* denotes the set of normalized features from training set \mathcal{D} . $kNN(z^*; \mathcal{D}^*)$ denotes the k-nearest neighbor of z^* in set \mathcal{D}^* .

Assume we have a feature encoder $\phi: \mathcal{X} \to \mathbb{R}^m$, and in training time we empirically observe n IND samples $\{\phi(\mathbf{x}_1), \phi(\mathbf{x}_2)...\phi(\mathbf{x}_n)\}$.

Analysis of the MD score. Denote Σ to be the covariance matrix of $\phi(x)$. The final feature we extract from data x is:

$$\boldsymbol{z}(\boldsymbol{x}) = A^{-1}\phi(\boldsymbol{x})$$

where $AA^T = \Sigma$. Note that the covariance of z is \mathcal{I} .

Given a class label c, we assume the distribution z(x|c) follows a Gaussian $\mathcal{N}(A^{-1}\mu_c,\mathcal{I})$. Immediately we have μ_c to be the class centroid for class c under the maximum likelihood estimation. We can now clearly address the relation between MD score and IND density (p(x)):

$$S_{MD}(\boldsymbol{x}) = 1/(-2 \max_{c \in \mathcal{V}} (\ln p(\boldsymbol{x}|c)) - m \ln 2\pi)$$

Analysis of KNN score. The normalized feature $z(x) = \phi(x)/||\phi(x)||_2$ is used for OOD detection. The probability density of z can be attained by:

$$p(\boldsymbol{z}) = \lim_{r \to 0} \frac{p(\boldsymbol{z}' \in B(\boldsymbol{z}, r))}{|B(\boldsymbol{z}, r)|}$$

where $B(z, r) = \{z' : ||z' - z||_2 \le r \land ||z'|| = 1\}$

Assuming each sample $z(x_i)$ is i.i.d with a probability mass 1/n, the density can be estimated by KNN distance. Specifically, $r=||z-k\mathit{NN}(z)||_2$, $p(z'\in B(z,r))=k/n$ and $|B(z,r)|=\frac{\pi^{(m-1)/2}}{\Gamma(\frac{m-1}{2}+1)}r^{m-1}+o(r^{m-1})$, where Γ is Euler's gamma function. When n is large and k/n is small, we have the following equations:

$$p(oldsymbol{x}) pprox rac{k\Gamma(rac{m-1}{2}+1)}{\pi^{(m-1)/2}nr^{m-1}}$$
 $S_{KNN}(oldsymbol{x}) pprox -(rac{k\Gamma(rac{m-1}{2}+1)}{\pi^{(m-1)/2}n})^{rac{1}{m-1}}(p(oldsymbol{x}))^{-rac{1}{m-1}}$

D ADDITIONAL DETAILS ABOUT TPLR

D.1 COMPUTATION OF THE MD SCORE

Mahalanobis distance score (MD) is an OOD score function initially proposed by Lee et al. (2018b), which is defined as:

$$S_{MD}(\boldsymbol{x}) = 1/\min_{c \in \mathcal{V}} \left((h(\boldsymbol{x}) - \boldsymbol{\mu}_c)^T \boldsymbol{\Sigma}^{-1} (h(\boldsymbol{x}) - \boldsymbol{\mu}_c) \right),$$

where h(x) is the feature extractor of a tested OOD detection model \mathcal{M} , μ_c is the centroid for a class c and Σ is the covariance matrix. The estimations of μ_c and Σ are defined by

$$oldsymbol{\mu}_c = rac{1}{N_c} \sum_{oldsymbol{x} \in \mathcal{D}_{train}^c} h(oldsymbol{x}),$$

$$\Sigma = \frac{1}{N} \sum_{c \in |\mathcal{Y}|} \sum_{\boldsymbol{x} \in \mathcal{D}_{vain}^c} (h(\boldsymbol{x}) - \boldsymbol{\mu}_c) (h(\boldsymbol{x}) - \boldsymbol{\mu}_c)^T,$$

where $\mathcal{D}^c_{train} := \{ \boldsymbol{x} : (\boldsymbol{x}, y) \in \mathcal{D}_{train}, y = c \}$, \mathcal{D}_{train} is the training set, N is the total number of training samples, and N_c is the number of training samples belonging to class c.

In the CIL setting, we have to compute μ_c and Σ for each task (assuming all classes in the task have the same covariance matrix) with trained task-specific model $\mathcal{M}^{(t)}$. Specifically, after training on the t-th task dataset $\mathcal{D}^{(t)}$, we compute:

$$\boldsymbol{\mu}_{c}^{(t)} = \frac{1}{N_{c}} \sum_{(\boldsymbol{x},c) \in \mathcal{D}^{(t)}} h(\boldsymbol{x}; \phi^{(t)}), \quad \forall c \in \mathcal{Y}^{(t)}$$
(18)

$$\Sigma^{(t)} = \frac{1}{|\mathcal{D}^{(t)}|} \sum_{c \in |\mathcal{Y}^{(t)}|} \sum_{(\boldsymbol{x},c) \in \mathcal{D}^{(t)}} (h(\boldsymbol{x};\phi^{(t)}) - \boldsymbol{\mu}_c^{(t)}) (h(\boldsymbol{x};\phi^{(t)}) - \boldsymbol{\mu}_c^{(t)})^T$$
(19)

We put the memory budget analysis of the saved class centroids $\mu_c^{(t)}$ and co-variance matrices $\Sigma^{(t)}$ in Appendix F.3.

D.2 COMPUTATION OF LOGIT-BASED SCORES

In Section 5.3, we compare the performance of TPLR with different logit-based scores MSP, EBO, and MLS. They are defined as follows:

$$S_{MSP}^{(t)}(\boldsymbol{x}) = \max_{i=1}^{|\mathcal{Y}_t|} softmax\left(f(h(\boldsymbol{x}; \phi^{(t)}); \theta^{(t)})\right)$$
(20)

$$S_{EBO}^{(t)}(\boldsymbol{x}) = \log \sum_{j=1}^{|\mathcal{Y}_t|} \left(\exp \left\{ f(h(\boldsymbol{x}; \phi^{(t)}); \theta^{(t)}) \right\} \right)$$
(21)

$$S_{MLS}^{(t)}(\boldsymbol{x}) = \max_{j=1}^{|\mathcal{Y}_t|} \left(f(h(\boldsymbol{x}; \phi^{(t)}); \theta^{(t)}) \right)$$
 (22)

In traditional OOD detection works, they are tested effective in estimating the probability of "x belongs to IND classes". Thus we can adopt them to design our TPLR method to estimate the probability of "x belongs to task t".

D.3 PSEUDO-CODE

To improve reproducibility, we provide the detailed pseudo-code for computing $S_{TPLR}(x)$ (using Equation (9) in the main text) as Algorithm 1. Then we give the pseudo-code for the CIL training as Algorithm 2 and testing for TPLR as Algorithm 3.

Algorithm 1 Compute TPLR Score with the t-th Task-specific Model $\mathcal{M}^{(t)}$

Input: Buf^* : replay buffer data without classes of task t; x: test sample; t: task-id; $\mathcal{M}^{(t)}$: the trained t-th task model $\mathcal{M}^{(t)}$ with feature extractor $h(x;\phi^{(t)})$ and classifier $f(x;\theta^{(t)})$; $\{\mu_c^{(t)}\}_{c\in\mathcal{Y}^{(t)}}$: pre-computed class centroids for task t; $\Sigma^{(t)}$: pre-computed covariance matrix for task t; k: KNN hyper-parameter; $1/\beta_1^{(t)}$: pre-computed empirical mean of $S_{MLS}(x)$; $1/\beta_2^{(t)}$: pre-computed empirical mean of $S_{MD}(x)$.

```
Return: TPLR Score S_{TPLR}(x)

1: S_{MLS}(x) \leftarrow \max_{c \in \mathcal{Y}^{(t)}} f(h(x; \phi^{(t)}); \theta^{(t)})_c

2: S_{MD}(x) \leftarrow 1/\left(\min_{c \in \mathcal{Y}^{(t)}} ((h(x; \phi^{(t)}) - \mu_c)^T \Sigma^{-1}(h(x; \phi^{(t)}) - \mu_c))\right)

3: S_{MLS}(x) \leftarrow S_{MLS}(x) * \beta_1^{(t)}

4: S_{MD}(x) \leftarrow S_{MD}(x) * \beta_2^{(t)}

5: z \leftarrow h(x; \phi^{(t)})/||h(x; \phi^{(t)})||_2

6: for \hat{x}_i in Bu/^x do

7: z_i \leftarrow h(\hat{x}_i; \phi^{(t)})/||h(\hat{x}_i; \phi^{(t)})||_2

8: d_i \leftarrow ||z_i - z||_2

9: end for

10: \{d_{ij}\}_{j=1}^{|Buf^*|} \leftarrow sorted(\{d_i\}_{i=1}^{|Buf^*|})

11: S_{TPLR}(x) \leftarrow -\log[\exp\{-S_{MLS}(x)\} + \exp\{-S_{MD}(x) - d_{i_k}\}]
```

Algorithm 2 CIL Training with TPLR

```
1: Initialize an empty replay buffer Buf
 2: for training data \mathcal{D}^{(t)} of each task do
          for each batch (x_i, y_i) \subset \mathcal{D}^{(t)} \cup \textit{Buf}, until converge do
               Minimize Eq.7 (in the main text) and update the parameters with HAT
 4:
 5:
          Compute \{\boldsymbol{\mu}_c^{(t)}\}_{c\in\mathcal{Y}^{(t)}} using Equation (18)
 6:
          Compute \Sigma^{(t)} using Equation (19)
 7:
          Compute 1/\beta_1^{(t)}, 1/\beta^{(t)} using Equation (10)
 8:
          Update Buf with \mathcal{D}^{(t)}
 9:
10: end for
11: Train the calibration parameters \{(\tilde{\sigma}_1^{(t)}, \tilde{\sigma}_2^{(t)})\}_{t=1}^T following Appendix A
```

Algorithm 3 CIL Testing with TPLR

```
Input: test sample \boldsymbol{x}
Return: predicted class \hat{c}

1: Compute S_{TPLR}(\boldsymbol{x};t) with each task model \mathcal{M}^{(t)} using Algorithm 1.

2: Preicition with Equation (3): \hat{c} = \arg\max_{c,t} \sigma_1^{(t)} \cdot \left\lceil softmax\left(f(h(\boldsymbol{x};\phi^{(t)});\theta^{(t)})\right)\right\rceil_i \cdot S(\boldsymbol{x};t) + \sigma_2^{(t)}
```

E DETAILS OF HAT

For completeness, we briefly describe the hard attention mechanism of HAT (Serra et al., 2018) used in TPLR. In learning the task-specific model $\mathcal{M}^{(t)}$ for each task, TPLR at the same time trains a *mask* for each adapter layer. To protect the shared feature extractor from previous tasks, their masks are used to block those important neurons so that the new task learning will not interfere with the parameters learned for previous tasks. The main idea is to use sigmoid to approximate a 0-1 gate function as *hard attention* to mask or unmask the information flow to protect parameters learned for each previous task.

The hard attention at layer l and task t is defined as:

$$a_{l}^{(t)} = sigmoid(s \cdot e_{l}^{(t)}),$$

where s is a temperature scaling term, $sigmoid(\cdot)$ denotes the sigmoid function, and $e_l^{(t)}$ is a *learnable* embedding for task t. The attention is element-wise multiplied to the output h_l of layer l as

$$oldsymbol{h}_l' = oldsymbol{a}_l^{(t)} \otimes oldsymbol{h}_l$$

The sigmoid function converges to a 0-1 binary gate as s goes to infinity. Since the binary gate is not differentiable, a fairly large s is chosen to achieve a differential pseudo gate function. The pseudo binary value of the attention determines how much information can flow forward and backward between adjacent layers. Denote $h_l = ReLU(W_lh_{l-1} + b_l)$, where $ReLU(\cdot)$ is the rectifier function. For neurons of attention $a_l^{(t)}$ with zero values, we can freely change the corresponding parameters in W_l and b_l without interfering the output h_l' . The neurons with non-zero mask values are necessary to perform the task, and thus need a protection for *catastrophic forgetting* (CF).

Specifically, during learning task t, we modify the gradients of parameters that are important in performing the previous tasks 1, 2, ..., t-1 so they are not interfered. Denote the accumulated mask by

$$\boldsymbol{a}_l^{(< t)} = \max(\boldsymbol{a}_l^{(< t - 1)}, \boldsymbol{a}_l^{(t - 1)}),$$

where $\max(\cdot, \cdot)$ is an element-wise maximum and the initial mask $\boldsymbol{a}_l^{(0)}$ is defined as a zero vector. $\boldsymbol{a}_l^{(< t)}$ is a collection of mask values at layer l where a neuron has value 1 if it has ever been activated previously. The gradient of parameter $w_{ij,l}$ is modified as

$$\nabla w_{ij,l}' = (1 - \min(a_{i,l}^{(< t)}, a_{j,l-1}^{(< t)})) \nabla w_{ij,l},$$

where $a_{i,l}^{(< t)}$ is the *i*-th unit of $\mathbf{a}_l^{(< t)}$. The gradient flow is blocked if both neurons *i* in the current layer and *j* in the previous layer have been activated. We apply the mask for all layers of adapters except the last layer. The parameters in last layer do not require protection as they are task-specific parameters.

A regularization is introduced to encourage sparsity in $a_l^{(t)}$ and parameter sharing with $a_l^{(< t)}$. The capacity of a network depletes when $a_l^{(< t)}$ becomes an all-one vector in all layers. Despite a set of new neurons can be added in network at any point in training for more capacity, we utilize resources more efficiently by minimizing the loss:

$$\mathcal{L}_{reg} = \frac{\sum_{l} \sum_{i} a_{i,l}^{(t)} (1 - a_{i,l}^{(< t)})}{\sum_{l} \sum_{i} (1 - a_{i,l}^{(< t)})},$$

The intuition of this term is to regularize the number of masked neurons. Then the loss of HAT defined as the second term from the R.H.S. of Eq (7) in the main text is:

$$\mathcal{L}_{HAT} = \mu \cdot \mathcal{L}_{reg}$$

where μ is a hyper-parameter to balance the optimization of classification objective and HAT regularization.

F IMPLEMENTATION DETAILS, NETWORK SIZE AND RUNNING TIME

F.1 IMPLEMENTATION DETAILS OF BASELINES

Datasets. We use three popular image datasets. (1) **CIFAR-10** (Krizhevsky & Hinton, 2010) consists of images of 10 classes with 50,000 / 10,000 training / testing samples. (2) **CIFAR-100** (Krizhevsky et al., 2009) consists of images with 50,000 / 10,000 training / testing samples. (3) **Tiny-ImageNet** (Le & Yang, 2015) has 120,000 images of 200 classes with 500 / 50 images per class for training / testing.

Implementation of CIL baselines (pre-trained setting). For CIL baselines, we follow the experiment setups as reported in their official papers unless additionally explained in Section 5.1. For the regularization hyper-parameter μ and temperature annealing term s (see Appendix E) used in HAT, we follow the baseline MORE and use $\mu=0.75$ and s=400 for all experiments as recommended in (Serra et al., 2018). For the approaches based on network expansion (DER, BEEF, FOSTER), we expand the network of adapters when using a pre-trained backbone. For ADAM, we choose the ADAM (adapter) version in their original paper, which is the best variant of ADAM. As some of the baselines are proposed to continually learn from scratch, we carefully tune **their hyper-parameters** to improve the performance to ensure a fair comparison. The implementation details of baselines under non-pre-training setting are shown in Appendix B.3.

Hyper-parameter tuning. Apart from β_1 and β_2 discussed in Section 5.3, the only hyper-parameters used in our method TPLR are γ , which is the temperature parameter for task-id prediction, and k, which is the hyper-parameter of $d_{KNN}(\boldsymbol{x}, \boldsymbol{Buf}^{\star})$ in Equation (7). The value of γ and k are searched from $\{0.01, 0.05, 0.10, 0.50, 1.0, 2.0, 5.0, 10.0\}$ and $\{1, 2, 5, 10, 50, 100\}$, respectively. We choose $\gamma = 0.05$, and k = 5 for all the experiments as they achieve the overall best results.

Training Details. To compare with the strongest baseline MORE and ROW, we follow their setup (Kim et al., 2022a; 2023) to set the training epochs as 20, 40, 15, 10 for CIFAR-10, CIFAR-100, T-5T, T-10T respectively. And we follow them to use SGD optimizer, the momentum of 0.9, the batch size of 64, the learning rate of 0.005 for C10-5T, T-5T, T-10T, C100-20T, and 0.001 for C100-10T.

F.2 HARDWARE AND SOFTWARE

We run all the experiments on NVIDIA GeForce RTX-2080Ti GPU. Our implementations are based on Ubuntu Linux 16.04 with Python 3.6.

F.3 COMPUTATIONAL BUDGET ANALYSIS

F.3.1 MEMORY CONSUMPTION

We present the network sizes of the CIL systems (with a pre-trained network) after learning the final task in Table 8.

With the exception of SLDA and L2P, all the CIL methods we studied utilize trainable adapter modules. The transformer backbone consumes 21.6 million parameters, while the adapters require 1.2M for CIFAR-10 and 2.4M for other datasets. In the case of SLDA, only the classifier on top of the fixed pre-trained feature extractor is fine-tuned as it requires a fixed feature extractor for all tasks, while L2P maintains a prompt pool with 32k parameters. Additionally, each method requires some specific elements (e.g., task embedding for HAT), resulting in varying parameter requirements for each method.

As mentioned in Appendix D.1, our method also necessitates the storage of class centroids and covariance matrices. For each class, we save a centroid of dimension 384, resulting in a total of 3.84k, 38.4k, and 76.8k parameters for CIFAR-10, CIFAR-100, and TinyImageNet, respectively. The covariance matrix is saved per task, with a size of 384×384 . Then the parameter count of covariance matrix can be computed by $T \times 384 \times 384$ for a dataset with T tasks. Consequently, the total parameter count is 737.3k, 1.5M, 2.9M, 737.3k, and 1.5M for C10-5T, C100-10T, C100-20T, T-5T, and T-10T, respectively. It is worth noting that this consumption is relatively small when compared to certain replay-based methods like iCaRL and HAL, which require a teacher model of the same size as the training model for knowledge distillation.

Table 8: Network size measured in the number of parameters (# parameters) for each method without the memory buffer.

	C10-5T	C100-10T	C100-20T	T-5T	T-10T
OWM	24.1M	24.4M	24.7M	24.3M	24.4M
ADAM	22.9M	24.1M	24.1M	24.1M	24.1M
PASS	22.9M	24.2M	24.2M	24.3M	24.4M
HAT	24.1M	24.4M	24.7M	24.3M	24.4M
SLDA	21.6M	21.6M	21.6M	21.7M	21.7M
L2P	21.7M	21.7M	21.7M	21.8M	21.8M
iCaRL	22.9M	24.1M	24.1M	24.1M	24.1M
A-GEM	26.5M	31.4M	31.4M	31.5M	31.5M
EEIL	22.9M	24.1M	24.1M	24.1M	24.1M
GD	22.9M	24.1M	24.1M	24.1M	24.1M
DER++	22.9M	24.1M	24.1M	24.1M	24.1M
HAL	22.9M	24.1M	24.1M	24.1M	24.1M
DER	27.7M	45.4M	69.1M	33.6M	45.5M
FOSTER	28.9M	46.7M	74.2M	35.8M	48.1M
BEEF	30.4M	48.4M	82.3M	37.7M	50.6M
MORE	23.7M	25.9M	27.7M	25.1M	25.9M
ROW	23.7M	26.0M	27.8M	25.2M	26.0M
TPLR	23.7	25.9M	27.7M	25.1M	25.9M

F.3.2 RUNNING TIME

The computation for our method TPLR is very efficient. It involves standard classifier training and likelihood raio score computation, which employed some OOD detection methods. The OOD score computation only involves mean, covariance computation, and KNN search, which are all very efficient with the Python packages scikit-learn⁷ and faiss⁸. We give the comparison in running time in Table 9. We use HAT as the base as MORE, ROW and TPLR all make use of HAT and MORE and ROW are the strongest baselines.

Table 9: Average running time measured in minutes per task (min/T) for three systems.

	C10-5T	C100-10T	C100-20T	T-5T	T-10T
HAT	17.8 min/T 20.6 min/T 21.8 min/T	17.6 min/T	9.4 min/T	28.0 min/T	9.48 min/T
MORE	20.6 min/T	23.3 min/T	11.7 min/T	32.8 min/T	11.2 min/T
ROW	21.8 min/T	25.2 min/T	12.6 min/T	34.1 min/T	11.9 min/T
TPLR	20.7 min/T	23.3 min/T	11.7 min/T	32.5 min/T	11.2 min/T

⁷https://scikit-learn.org/stable/

⁸https://github.com/facebookresearch/faiss

G LIMITATIONS

Here we discuss the limitations of our proposed method TPLR.

First, our TPLR relies on replay, which may affect privacy in some situations and needs extra storage. We will explore how to improve task-id prediction methods in CIL setting without replay in the future. **Second,** TPLR uses a naive saving strategy that saves task data randomly to the replay buffer for simplicity. We may also consider better buffer saving strategies in the future. **Third,** this paper focuses on the traditional *offline* CIL problem set-up. In this mode, all the training data for a task is available upfront and the training can take any number of epochs. Also, the label space $\mathcal{Y}^{(t)}$ of different tasks are disjoint. We also notice that there are various studies that introduces different kinds of CIL settings, such as (1) *Online Continual Learning* (Guo et al., 2022), where data comes in a stream, and (2) *Blurry Task Setting* (Bang et al., 2022), where the incoming data labels may overlap. It is an exciting direction for our future works to see how to adapt our method to exploit the specific information in these settings.